



Archaeal community composition in Holocene methane pockmarks of the Gdańsk Basin (Baltic Sea, Poland): insights from tetraether lipids and 16S rRNA analysis

Izabela De Mey-Śnieżyńska¹, Mirosław Słowakiewicz¹, Francien Peterse², Aleksandra Brodecka-Goluch⁴, Andrzej Borkowski³, and Katarzyna Łukawska-Matuszewska⁴

¹University of Warsaw, Faculty of Geology, 02-089 Warsaw, Poland

²Utrecht University, Department of Earth Sciences, 3584 CS Utrecht, The Netherlands

³AGH University of Krakow, Faculty of Geology, Geophysics and Environmental Protection, 30-059 Kraków, Poland

⁴University of Gdańsk, Faculty of Oceanography and Geography, 81-379 Gdynia, Poland

Correspondence: Izabela De Mey-Śnieżyńska (i.sniezynska@uw.edu.pl)

Received: 30 January 2026 – Discussion started: 4 February 2026

Revised: 15 June 2026 – Accepted: 17 June 2026 – Published: 6 July 2026

Abstract. Methane pockmarks and shallow gas systems are prominent geomorphological features in the Baltic Sea that act as hotspots of microbial activity. In the Gdańsk Basin, pockmarks vary in gas-seepage intensity and in the extent of freshened porewater discharge, both of which influence the archaeal community structure and the composition of internal methane biofilters. The objective of this study was to examine the effects of methane seepage and freshened porewater on the composition of archaeal communities and on the isoprenoid glycerol dialkyl glycerol tetraethers (iGDGTs), membrane lipids synthesised by these communities, across the gas systems examined. Additionally, the effects of these environmental factors on the use and interpretation of iGDGT-based proxies under conditions of gas and water seepage were assessed. The study investigates whether iGDGT patterns in these Baltic gas systems reflect methane-driven processes, including anaerobic oxidation of methane (AOM) and methanogenesis, porewater freshening, or pelagic contributions from ammonia-oxidising archaea (AOA). The results show elevated iGDGT concentrations in pockmark cores compared with reference non-pockmark cores; however, the summed iGDGT concentration varies by site. Overall, iGDGT concentrations are much higher at sites with reduced seabed pockmark activity and weak porewater freshening. Nevertheless, consistently low Methane Index values (MI < 0.09), together with low GDGT-0 / crenarchaeol (< 1) and low GDGT-2 / cren

(< 0.04) ratios, indicate that the iGDGT pool lacks the typical enrichment in GDGT-1 to -3 associated with AOM, suggesting no AOM imprint on the iGDGT pool. However, 16S rRNA analysis revealed that the anaerobic methanotrophic archaeal lineages (ANME) consist of ANME-2b and ANME-3. A strong positive correlation between OH-GDGTs and crenarchaeol, together with the consistency of OH-GDGT% values with those previously reported for Baltic Sea surface sediments, suggests a thaumarchaeal source of iGDGTs in the studied pockmark and reference cores. The Branched and Isoprenoid Tetraether (BIT) index values suggest marine archaeal GDGT production. In this system, iGDGT-based proxies primarily reflect a strong pelagic presence of AOA, as indicated by the dominance of crenarchaeol. This suggests that, despite the local presence of methanogenic and ANME-related archaeal groups, methane-related AOM does not influence the iGDGT signal due to the archaeal community structure. These findings highlight the complex interplay between freshened porewater and gas seepage in shaping archaeal communities, and the role of ammonia-oxidising Nitrososphaeria in controlling iGDGT composition and the sedimentary record.

Highlights.

- Pockmark sediments harbour substantially higher archaeal diversity and abundance than non-pockmark reference sediments.
- The P/MET4 pockmark in the Gdańsk Deep hosts the most diverse and abundant methanogen community, coinciding with the highest concentrations of isoprenoid glycerol dialkyl glycerol tetraether lipids (iGDGTs).
- Crenarchaeol dominates the iGDGT pool in both pockmark and reference sediment cores, indicating strong Nitrososphaeria-related iGDGT synthesis in the water column.

1 Introduction

Pockmarks are concave geological structures ranging from a few metres up to several hundred metres in width and up to 100 m in depth, formed by gas and/or water seepage from the sediments into the hydrosphere (King and MacLean, 1970; Hovland and Judd, 1988). As indicators of hydraulic activity, they are categorised as active or inactive depending on whether gas and/or water seepage is continuous or dormant/intermittent (Hovland and Judd, 1988; Hovland et al., 2002). Their morphology facilitate detection through geophysical and hydroacoustic surveys, making pockmarks practical proxies for investigating seepage phenomena (Hovland and Judd, 1988), which occur globally on continental shelves and margins, including off Nova Scotia (King and MacLean, 1970), thousands of newly discovered pockmarks offshore California (Lundsten et al., 2024), in the Gulf of Mexico (Roberts and Aharon, 1994; Lawal et al., 2026). The formation of pockmarks requires pressure buildup in fine-grained, low-permeability sediments, with methane (CH₄) as the most commonly emitted component because of its high mobility (Hovland and Judd, 1988). Seepage types vary globally and include biogenic, thermogenic, or hydrothermal gas seepage; groundwater; or combined gas-and-water seepage (Hovland and Judd, 1988). Pockmarks predominantly form along salt-dome margins (Schmuck and Paull, 1993; Taylor et al., 2000) and in dislocation zones, faults, and bedrock fractures (Shaw et al., 1997). They also occur in regions of low seismicity, such as Sweden (Hovland et al., 2002) and the southern Baltic Sea (Idczak et al., 2020). Glacial and post-glacial processes can influence their formation by generating overpressure, as observed in the North Sea (Callow et al., 2021) and the Baltic Sea (Whiticar and Werner, 1981; Whiticar, 2002; Kreuzburg et al., 2023). Baltic Sea pockmarks have been documented in Eckernförde Bay and the Mecklenburg Bight (Werner, 1978; Wever et al., 1998; Jensen et al., 2002; Schlüter et al., 2004; Hoffmann et al., 2020; Díaz-Mendoza et al., 2023), the Stockholm Archipelago (Jakobsson et al., 2020), offshore Finland (Virtasalo et al., 2019), and the Gdańsk Basin (Pimenov et al., 2010; Majewski and Klusek, 2011; Brodecka et al., 2013;

Jaśniewicz et al., 2019; Idczak et al., 2020; Brodecka-Goluch et al., 2022). The Gdańsk Basin is the focus of this study.

In several Baltic settings, pockmarks have been linked to submarine groundwater discharge (SGD), broadly defined as the movement of fresh, brackish, or saline groundwater into the sea or ocean across the sediment-water interface. SGD encompasses both the inflow of freshened groundwater and the recirculation of saline porewater or seawater, driven by hydraulic pressure and density differences (Burnett et al., 2003, 2006; Moore, 2010; Taniguchi et al., 2019). Evidence of an association between pockmarks and upward groundwater infiltration has been documented in areas such as Eckernförde Bay (Bussmann and Suess, 1998; Schlüter et al., 2004), Hanko Bay (Virtasalo et al., 2019; Purkamo et al., 2022), and the central Gulf of Gdańsk (Szymczycha et al., 2016; Idczak et al., 2020). In the Gdańsk Basin area (Fig. 1), deep-water, fine-grained pockmarks are associated with localised porewater freshening, indicated by chloride (Cl⁻) and sulphate (SO₄²⁻) depletion, linked to seepage of freshened groundwater or discharge of freshened porewater (Szymczycha et al., 2018; Idczak et al., 2020; Brodecka-Goluch et al., 2022; Kurowski et al., 2024; Łukawska-Matuszewska and Dwornik, 2025; Łukawska-Matuszewska et al., 2025). The impact of SGD discharge on pockmark sediments depends on the source, chemical composition, and flow regime of the discharging fluids. Nevertheless, freshened SGD and associated porewater transport can alter the distribution of dissolved species, including NH₄⁺, CH₄, dissolved inorganic carbon (DIC), H₂S, Cl⁻, and SO₄²⁻, thereby shifting redox transition zones and influencing CH₄ cycling (Schlüter et al., 2004; Liu et al., 2017; Idczak et al., 2020; O'Reilly et al., 2021; Brodecka-Goluch et al., 2022; Zhang et al., 2025). In the pockmarks of Gdańsk Basin, Cl⁻ and SO₄²⁻ depletion linked to freshened porewater discharge may weaken SO₄²⁻-driven anaerobic methane oxidation (S-AOM), promote shallow methanogenesis, and contribute to episodic gas release into the water column (Idczak et al., 2020).

At the sulphate-methane interface (SMI), where the sub-seafloor intersection of downward-diffusing sulphate and upward-diffusing CH₄ occurs, ascending CH₄ is consumed in AOM (Zehnder and Brock, 1980; Boetius et al., 2000). It is mediated by sulphate-reducing bacteria (SRB) and anaerobic methanotrophic archaea (ANME) (Knittel and Boetius, 2009), which limit CH₄ emissions to the water column (Reeburgh, 2007). In the Baltic Sea, a halocline at 60–80 m separates oxygenated and anoxic waters, structuring key biogeochemical cycles (Kuliński et al., 2022), including an oxic-suboxic nitrogen-cycling zone driven by ammonia-oxidising archaea (AOA) (Berg et al., 2015b; Jäntti et al., 2018). Archaeal biomarkers for methane cycling (ANME, methanogens) and nitrification (AOA), such as intact polar GDGTs (IPL-GDGTs), can be transported and preserved as core isoprenoidal GDGTs (CL-iGDGTs) in sediments (Schouten et al., 2013).

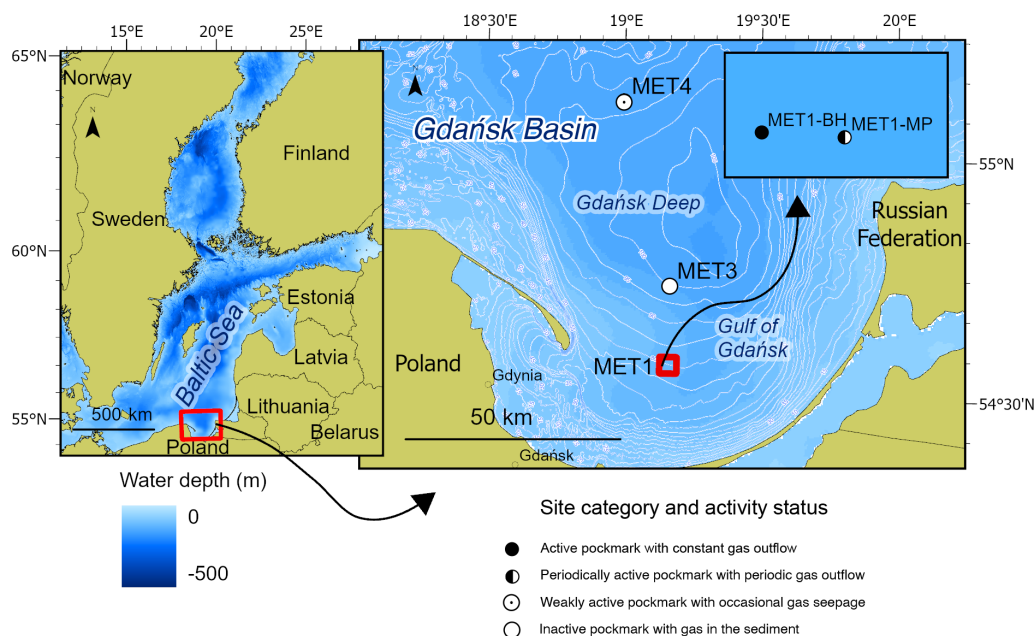


Figure 1. Map of the study area in the south-eastern Baltic Sea, the Gdańsk Basin. The main panel shows the Gdańsk Basin, including the Gdańsk Deep and the Gulf of Gdańsk. Symbols indicate the category and activity status of the investigated pockmark sites (tagged with a “P” prefix) with respect to venting status, based on MBES and SBES observations collected during the present and previous research campaigns in 2019–2025. Reference stations (labelled as surrounding stations and tagged with an “S” prefix) are referred to as non-pockmark cores or reference cores. They are positioned approximately 100–150 m from the corresponding pockmark margins on morphologically regular seafloor lacking pockmark depressions; they are not shown separately on the map due to the map’s scale. Additional data, including $\text{CH}_4/\text{SO}_4^{2-}$ profiles and Cl^- profiles, are presented in Figs. 2 and 3, respectively. More detailed data, for example, concerning porewater freshening, are available in the Supplement (Table S1). Map source: Eurostat/GISCO, 2024, scale 1.

Archaeal iGDGTs are membrane lipids whose structures adapt to environmental changes (De Rosa et al., 1977; Huguet et al., 2006; Liu et al., 2017; Schouten et al., 2002, 2013; Sinninghe Damsté et al., 2022). In marine sediments, GDGT-0 and crenarchaeol dominate. Crenarchaeol is produced by Thaumarchaeota (Sinninghe Damsté et al., 2002) – in current nomenclature, Nitrososphaeria, class of Thermo-*proteota* phylum (Rinke et al., 2021). Nitrososphaeria are the main ammonia oxidisers (Berg et al., 2015a, b) and iGDGT synthesisers in the Baltic Sea (Labrenz et al., 2010; Wittenborn et al., 2023). Methanogens primarily produce GDGT-0, whereas methanotrophs, mainly ANME-1, produce GDGT-1 to -3 (Koga et al., 1993; Pancost et al., 2001; Weijers et al., 2006; Rossel et al., 2008; Blaga et al., 2009; Zhang et al., 2011; Inglis et al., 2015; Słowakiewicz et al., 2016; Petrick et al., 2019). Hydroxylated-GDGTs (OH-GDGTs) are produced primarily by Thaumarchaeota (Sinninghe Damsté et al., 2002; Liu et al., 2012; Kaiser and Arz, 2016; Elling et al., 2017; Bale et al., 2019; Sinninghe Damsté et al., 2022), but can also be biosynthesised by methanogens or ANME (Liu et al., 2012; Guan et al., 2024; Fenies et al., 2026). OH-GDGT synthesis reflects cold adaptation (Liu et al., 2012) and salinity changes (Sinninghe Damsté et al., 2022); OH-GDGT-0 is most abundant at high latitudes (Huguet et al., 2013; Varma et al., 2024) and in Baltic Sea sediments, where

culture studies have confirmed an AOA source (Blainey et al., 2011; Berg et al., 2015a).

Groundwater-seawater mixing zones in permeable coastal aquifers are commonly conceptualised as subterranean estuaries (Moore, 1999; Ruiz-González et al., 2021). This conceptual framework is useful for SGD-affected systems because microbial activity within these mixing zones can modify the chemical composition of groundwater before it reaches the seabed (Ruiz-González et al., 2021). Importantly, deeper groundwater mixing zones have been reported to host distinct archaeal communities, including AOA populations (Santoro et al., 2008; Rogers and Casciotti, 2010; Purkamo et al., 2022; Wilson et al., 2024). Therefore, in addition to pelagic and sedimentary sources, groundwater-associated archaeal communities should be considered as a potential source of archaeal tetraether lipids in SGD-influenced marine sediments. This is particularly relevant for Baltic Sea pockmarks, where iGDGTs may reflect several partly overlapping sources and processes. In the Baltic Sea water column, iGDGTs and OH-GDGTs are mainly associated with Nitrososphaeria, especially *Candidatus Nitrosopumilus*, inhabiting the pelagic redoxcline (Sinninghe Damsté et al., 2022; Wittenborn et al., 2023). However, GDGT-0 can also be produced by methanogenic archaea, which are expected to contribute to CH_4 production in the studied pockmark sedi-

ments. Moreover, although direct studies of GDGTs in SGD-affected marine sediments remain scarce, groundwater studies show that both CL-iGDGTs and IPL-iGDGTs can be produced in situ by indigenous subsurface microbial communities, with distributions linked to groundwater thaumarchaeotal groups rather than solely to allochthonous surface inputs (Ding et al., 2018). Consequently, in methane pockmark sediments affected by porewater freshening, archaeal 16S rRNA and CL-iGDGT distributions may record multiple controls: the regional input of Baltic pelagic AOA, sedimentary CH₄-driven processes including methanogenesis and methanotrophy, and a hydrogeochemical imprint associated with freshened porewater or SGD-related seawater-groundwater mixing. Because OH-GDGT distributions are also sensitive to salinity changes (Sinninghe Damsté et al., 2022), these compounds may be responsive to porewater freshening in the examined pockmarks. Thus, the studied system provides a natural setting to test whether archaeal tetraether lipids primarily reflect pelagic marine production, sedimentary methane cycling, or additional influence from freshened porewater.

2 Materials and methods

2.1 Study area

Pockmarks in the Gdańsk Deep and the central Gulf of Gdańsk (Fig. 1) occur at water depths of 1–100 m and are characterised by active gas seepage from Holocene silts and clays (Idczak et al., 2020). Although the gas is predominantly biogenic (Brodecka-Goluch et al., 2022), the presence of helium (up to 0.39 %) (Idczak et al., 2020) and noble gases (Ne, Ar, Kr, Xe) (Brodecka-Goluch et al., 2022) in samples from station MET1 suggests that these pockmarks vent Middle Cambrian reservoirs, with gas migrating through sedimentary layers along faults (Jaworowski et al., 2010; Idczak et al., 2020; Brodecka-Goluch et al., 2022), possibly with additional contributions from the crust and mantle (Kotarba, 2010; Pokorski, 2010; Kotarba and Lewan, 2013; Kotarba and Nagao, 2015).

The study area spans the Gdańsk Basin and includes stations MET3 and MET4 in the northern Gdańsk Deep, and MET1-MP and MET1-BH in the Gulf of Gdańsk (Fig. 1). The southern stations (MET1 area) receive a high input of terrestrial organic matter from the Vistula River, trap plant material and organic debris, and experience moderate anthropogenic contamination, resulting in elevated total organic carbon (TOC) (Idczak et al., 2020; Brodecka-Goluch et al., 2022; Łukawska-Matuszewska et al., 2022; Szymczak-Żyła and Lubecki, 2022). Sedimentation rates are lower in MET3 and MET4 ($\sim 0.17\text{--}0.20\text{ cm yr}^{-1}$) than at MET1 ($\sim 0.15\text{--}0.22\text{ cm yr}^{-1}$) (Szczyńska and Uścińowicz, 1994; Brodecka-Goluch et al., 2022). In a previous study of pockmarks in the Gdańsk Deep, Brodecka-Goluch et al. (2022) reported that CH₄ at pockmark P/MET3 has isotopic signatures

of marine microbial gas, whereas gas venting from MET1-MP shows mixed marine and terrestrial signatures, indicating the upward infiltration of freshwater. Thus, methanogenic pathways vary between sites: acetoclastic at MET1-BH, hydrogenotrophic at MET3, and mixed at MET1-MP (Idczak et al., 2020; Brodecka-Goluch et al., 2022). The MET1 pockmarks are characterised by intensive/periodic gas and freshwater seepage (Idczak et al., 2020; Brodecka-Goluch et al., 2022). MET4 represents the least-studied system, located within a field of multiple pockmarks (Brodecka-Goluch et al., 2020).

In the Gdańsk Basin, SGD is divided into shallow/coastal and deep/offshore components. The shallow/coastal component occurs in nearshore areas and is fed by Quaternary-Cretaceous coastal aquifers (e.g., Piekarek-Jankowska, 1996; Szymczycha et al., 2016, 2018). By contrast, the deep/offshore component comprises artesian-type freshwater seepage with episodic discharge at deep-water pockmarks such as MET1 (Szymczycha et al., 2018; Idczak et al., 2020). Deep SGD originates from extensive Upper Cretaceous aquifers beneath the Gulf of Gdańsk (Uścińowicz, 2011). Seepage intensity varies with hydrostatic pressure, water-column processes, and fault activity (Brodecka-Goluch et al., 2022). After commercial extraction ceased in 2000, natural hydrodynamic conditions returned (Uścińowicz, 2011), although the extent and periodicity of deep discharge remain unquantified. SGD in the MET1 area reduces sulphate and chloride concentrations with depth, thereby compressing the SMI to a few cm below the seafloor (Idczak et al., 2020; Brodecka-Goluch et al., 2022; Łukawska-Matuszewska and Dwornik, 2025). A high carbonate alkalinity flux at MET1-MP indicates substantial DIC generation during anaerobic diagenesis, potentially linked to Fe(III)-AOM (Łukawska-Matuszewska and Dwornik, 2025). The near-bottom chloride concentration in the Gulf of Gdańsk ranges from 150 to 180 mmol L⁻¹, equivalent to $\sim 5318\text{--}6384\text{ mg dm}^{-3}$ (Łukawska-Matuszewska, 2016). For the Gdańsk Deep, the mean value is approximately 12 PSU, equivalent to 6700–6900 mg dm⁻³ (Kapustina et al., 2026).

2.2 Sampling at MET stations

The research stations were divided into pockmarks (morphologically concave geological structures with gas emissions to the water column and/or gas-bearing sediments with possible SGD) and references (non-pockmark reference sites with gas in the sediments but without emission to the water column or SGD). Pockmark stations were further classified (see Table S1 in the Supplement) based on previous studies, including hydroacoustic and geophysical investigations (Brodecka-Goluch et al., 2020, 2022; Idczak et al., 2020), as well as data included in this study (SO₄²⁻ and CH₄ profiles: Fig. 2; Cl⁻ profiles: Fig. 2; echograms for pockmarks P/MET3 and P/MET4: Fig. S1), as active (gas emission to the water column, influence of freshened porewater, or both:

P/MET1-BH, P/MET1-MP), weakly active (gas seepage and porewater freshening: P/MET4), or inactive (gas present in the sediments without clear emission or freshwater seepage: P/MET3).

Eight 95 cm-long sediment cores were collected from the central parts of methane-seeping structures in the central Gdańsk Basin (south-eastern Baltic Sea) using a gravity corer at three areas and four study locations (MET1: MET1-MP, MET1-BH; MET3; MET4; Fig. 1, Table S1) during a cruise aboard RV *Oceanograf* (University of Gdańsk) in October 2019. Four additional cores were collected from outside the pockmarks (~ 100–150 m away) as reference samples. Samples were categorised by origin: a “P” prefix (P/METX; X = 1-MP, 1-BH, 3, 4) for pockmark sediments and an “S” prefix (S/METX) for surrounding sediments, namely reference non-pockmark sediments.

Onboard, the 95 cm cores for biomarker analysis were sectioned into a top 0–5 cm interval and subsequent 10 cm intervals (hereafter referred to as horizons) for the remainder of the cores, yielding 72 samples for geochemical analysis (some bottom samples are missing). Samples for microbial analysis were subsampled at a slightly coarser 1 cm resolution from the top (1), mid-depth (5), and bottom (7, 10) intervals using a sterile spatula.

2.3 Porewater sampling

Porewater samples were collected under anoxic conditions from intact, hermetically sealed sediment cores using Rhizon® samplers. Sediment subsamples for CH₄ determination were collected immediately after core retrieval. Sampling was performed through pre-drilled holes in the core liners using 3 mL syringes (with the Luer tip removed), and the material was immediately transferred into 20 mL vials in accordance with the protocol described by Jørgensen et al. (2001). Chloride and SO₄²⁻ concentrations in porewater were measured by high-performance ion chromatography (Metrohm 850 Professional IC) with analytical precision better than 3%. Methane concentrations were determined by the standard headspace technique using a gas chromatograph (Perkin-Elmer) equipped with a flame ionisation detector (FID) and an HP-5 capillary column (30 m × 0.32 mm × 0.25 μm), with helium as the carrier gas. The method detection limit (LOD) was 0.2 μmol dm⁻³. Measured CH₄ concentrations were corrected for sediment porosity. Porosity for each sample was calculated from water and organic matter contents (LOI; see below) using the equations of Engvall (1978) and Carman and Jonsson (1991).

2.4 LOI analysis

The organic matter content was assessed by gravimetric loss-on-ignition (LOI) after dehydration (105 °C for 24 h) and dry combustion (550 °C for 6 h). Łukawska-Matuszewska et al. (2014) previously demonstrated the applicability of LOI in

the Gdańsk Basin as a proxy for sedimentary organic matter content. LOI-based values were additionally evaluated against directly measured TOC for two pockmark and reference representative cores. TOC content in sediments was measured using a CHNS autoanalyser (Perkin Elmer 2400) following Parsons et al. (1984). For TOC analysis, samples were acidified with 1 M HCl to remove inorganic carbon, following Hedges and Stern (1984).

2.5 Tetraether lipid extraction and analysis

All freeze-dried samples were ground with a mortar and pestle. Approximately 1 g of each sample was extracted with dichloromethane : methanol (DCM : MeOH, 2 : 1, v/v) in an ultrasonic water bath. Total lipid extracts (TLEs) were chromatographed on a silica gel column with *n*-hexane and methanol as eluents to obtain apolar and polar fractions, respectively.

The polar fraction containing core GDGTs was redissolved in hexane / isopropanol (99 : 1, v/v), spiked with a known amount of an internal standard (a C₄₆ glycerol trialkyl glycerol tetraether; Huguet et al., 2006), and filtered through a 0.45 μm polytetrafluoroethylene syringe filter. GDGTs were analysed at Utrecht University using an ultra-high-performance liquid chromatograph (UHPLC; Agilent 1260 Infinity) coupled to an Agilent 6130 single-quadrupole mass detector, following the method proposed by Hopmans et al. (2016). Quantification was performed by manually integrating the peak areas of the protonated ions ([M+H]⁺) in ChemStation software (B.04.03), and the results were compared with those of the internal standard. Selected ion monitoring (SIM) was used to detect and identify GDGTs. The target ions were *m/z* 1302, 1300, 1298, 1296 and 1292 for iGDGTs and OH-GDGTs.

Absolute GDGT concentrations were calculated relative to the C₄₆ internal standard and sediment dry weight, following established GDGT quantification approaches (Huguet et al., 2006, 2010), and are therefore reported as semi-quantitative concentrations (Bijl et al., 2025). Derived fractional abundances and GDGT-based indices were calculated from the integrated peak areas. Raw peak areas, derived fractional abundances and indices, and semi-quantitative absolute concentrations are reported in accordance with the GDGT data-reporting recommendations of Bijl et al. (2025).

Each sediment horizon was analysed once. Replicate analyses were not available for individual horizons. Therefore, sample-specific analytical uncertainty could not be estimated, and error bars are not shown in the downcore plots. Method uncertainty includes peak integration, instrumental response, extraction/processing effects, and the semi-quantitative nature of C₄₆-based concentration estimates (Bijl et al., 2025).

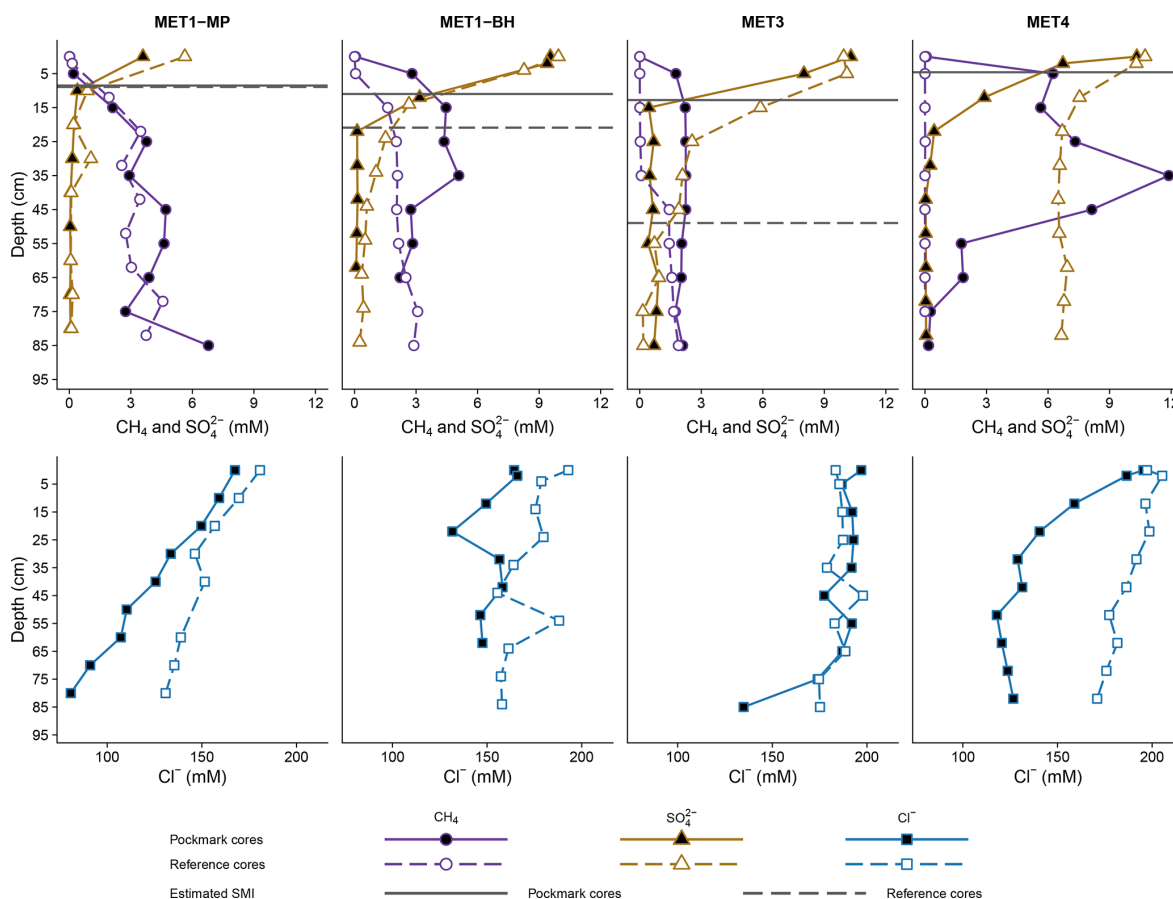


Figure 2. Profiles of SO_4^{2-} and CH_4 differ in absolute concentrations across sites, with greater SO_4^{2-} depletion occurring closer to the surface in pockmarks than in reference sites. Methane concentrations are, on average, approximately 2.3 times higher in pockmark cores than in reference cores, with the highest values at P/MET4. Dashed (reference cores) and solid (pockmark cores) horizontal lines indicate the SMI estimated at the point where porewater concentrations of SO_4^{2-} and CH_4 are equal. Depth profiles of porewater Cl^- at MET1-MP, MET1-BH, MET3, and MET4, ranging from 2863 to 7279 mg dm^{-3} . The profiles consistently show higher Cl^- concentrations in reference sediments than in those in pockmark sediments. The extent and shape of these profiles vary across sites. The most distinct separation between pockmark and reference profiles occurs at MET4 and MET1-MP, whereas MET3 shows substantial overlap. Depth is given in cm below the sea floor (bsf).

2.6 DNA isolation, sequencing, and data analysis

Genomic DNA from the sediment samples was isolated using the EURx kit for complex matrices (Soil DNA Purification Kit, no. E3570, EURX Ltd., Poland). The protocol requires mechanical homogenisation to release cells from the sediment matrix. The isolated genomic DNA was subjected to metabarcoding analysis. Sequencing of the hypervariable V3–V4 region of the 16S rRNA gene was outsourced to GENOMED S.A. (Warsaw, Poland). Specific primer sequences (developed by Zymo Research, CA, USA) were used to amplify the selected region and prepare libraries (341F: CCTACGGGDCGCWGCAG, CCTAYGGGGYGCWGCAG; 806R: GACTACNVGGGTMTCTAATCC).

PCR was performed using Q5 Hot Start High-Fidelity $2 \times$ Master Mix, with reaction conditions in accordance with

the manufacturer's recommendations. Sequencing was performed on a MiSeq sequencer using paired-end (PE) technology (2×300 nt) with Illumina's v3 kit. FASTQ files were processed with *fastp* (v. 0.23.2) (Chen et al., 2018) to improve raw sequence quality by trimming adapters, filtering low-quality reads, and removing artefacts. The sequences were further analysed using Kraken2 (Wood et al., 2019) following the protocol described by Lu et al. (2022). The SILVA database (v. 138) was used for taxonomic assignment (Quast et al., 2013). Bracken was then applied to the Kraken2 reports, set to the genus level with a threshold of five (Lu et al., 2017). The resulting data were transformed before analysis. To address zero values, the data were imputed using the R package *Compositions* (v. 1.4.0.1) (Palarea-Albaladejo and Martín-Fernández, 2015). The centred log-ratio (clr) transformation was then applied using the *Compositions* package

for R (v. 2.05; Aitchison, 1982; Quinn et al., 2019; van den Boogaart et al., 2024).

Taxonomic names are reported according to the database classification used in the bioinformatic workflow. The Deep Sea Euryarchaeotic Group (DSEG) is therefore retained when returned by the database, although this lineage is classified within Thermoplasmata in newer phylogenetic classifications (Rinke et al., 2021).

2.7 Statistical analysis and data visualisation

Multidimensional analyses, correlograms, and hierarchical analyses were conducted using R (R Core Team, 2022). RStudio 2025.05.0+496 “Mariposa Orchid” and R version 4.3.3 (2024-02-29) on the x86_64-apple-darwin20 (64-bit) platform were used for all analyses. A heatmap of the archaeal community (at the class level) with cluster analysis was generated using the Heatmap function in the *ComplexHeatmap* package. To examine the grouping of samples between pockmark and reference sites, Classical Multidimensional Scaling (MDS; principal coordinates analysis) was performed using the `dist` function (`dist_matrix <- dist(data, method = “euclidean”)`) and the `cmdscale` function (`mds <- cmdscale(dist_matrix)`) from the *stats* package. The MDS results were visualised using the *ggplot2* and *ggrepel* packages (Wickham, 2016).

Permutational Multivariate Analysis of Variance (PERMANOVA) was conducted using `adonis2` (`permutations = 999, method = “bray”`) in the *vegan* package. Principal Component Analysis (PCA) was conducted using the *FactoMineR* package, and the results were visualised with `fviz_pca_var` from the *factoextra* package. A correlation network illustrating relationships between Archaea (at the family taxonomic level) and GDGTs was constructed using `cor` from the *stats* package; `graph_from_adjacency_matrix` (`mode = “undirected”, weighted = TRUE, diag = FALSE`) from the *igraph* package; `mutate_as_tbl` from the *tidygraph* package; and *ggraph* for visualisation. Community structure was identified using `group_louvain` (multilevel optimisation of modularity via `igraph::cluster_louvain()`), which implements the multi-level modularity optimisation algorithm described by Blondel et al. (2008). Cross-correlations between iGDGT and OH-GDGT concentrations were calculated in R using `stats::cor.test()` with Pearson correlation. Concentrations were \log_{10} -transformed ($\log_{10}[x + 10^6]$) before correlation analysis to reduce right skew. Correlations were computed using pairwise complete observations. To correct for multiple testing, *p*-values were adjusted using the Benjamini–Hochberg false discovery rate (FDR) procedure.

2.8 Calculation of indices

The GDGT-0/crenarchaeol ratio was calculated to assess potential contributions to iGDGT production from methanogens (although GDGT-0 is not exclusive to them)

and ammonia-oxidising archaea (Blaga et al., 2009). Values > 2 have been proposed to indicate a substantial methanogenic input (Blaga et al., 2009; Schouten et al., 2013; Zell et al., 2014).

$$\text{GDGT-0/cren} = [\text{GDGT-0}]/[\text{crenarchaeol}] \quad (1)$$

The GDGT-2 / crenarchaeol (GDGT-2 / cren) index is used as an additional screening tool to assess a potential AOM contribution (Weijers et al., 2011). An elevated GDGT-2 / cren ratio suggests increased synthesis of GDGT-2 within the SMI, likely from methanotrophic Euryarchaeota (Pancost et al., 2001; Wakeham et al., 2003; Stadnitskaia et al., 2005).

$$\text{GDGT-2/cren} = [\text{GDGT-2}]/[\text{crenarchaeol}] \quad (2)$$

The Methane Index (MI) is based on GDGT-1 to GDGT-3 and crenarchaeol, and reflects the balance between methanotrophic Euryarchaeota and Nitrososphaeria, planktonic or benthic (Zhang et al., 2011). GDGTs associated with methanotrophs – mainly GDGT-1 to GDGT-3 (Pancost et al., 2001; Zhang et al., 2011) – are primarily produced by ANME-1 (Rossel et al., 2008). The MI ranges from 0 to 1, with higher values (> 0.3 – 0.5) indicating a greater relative contribution of GDGT-1 to GDGT-3 than of crenarchaeol and cren', and are linked to high methane fluxes (Kim and Zhang, 2023). The MI, as defined by Zhang et al. (2011), was calculated as follows:

$$\text{MI} = \frac{[\text{GDGT-1} + \text{GDGT-2} + \text{GDGT-3}]}{[\text{GDGT-1} + \text{GDGT-2} + \text{GDGT-3} + \text{cren} + \text{cren}']} \quad (3)$$

The Branched and Isoprenoid Tetraether index (BIT) estimates the relative contribution of branched GDGTs (brGDGTs) to the combined pool of brGDGTs and crenarchaeol, following Hopmans et al. (2004), and serves as an indicator of terrestrial organic matter input into a marine environment. However, brGDGTs may also be produced in situ in aquatic and sedimentary environments (Peterse et al., 2009; Dearing Crampton-Flood et al., 2019, and references therein). The BIT index ranges from 0 to 1, with higher values indicating a greater relative contribution of brGDGTs compared with crenarchaeol:

$$\text{BIT} = \frac{[\text{brGDGT-Ia} + \text{II-a} + \text{IIIa}]}{[\text{br-GDGT-Ia} + \text{IIa} + \text{IIIa} + \text{cren}]} \quad (4)$$

The percentage of OH-GDGTs reflects the relative contribution of hydroxylated iGDGTs to the total iGDGT pool and indicates an increased contribution from OH-GDGT-producing archaea and/or adaptation to low temperature and salinity.

The index was calculated following Huguet et al. (2013):

$$\begin{aligned} \text{OH-GDGT}\% = & \frac{\Sigma[\text{OH-GDGT-0} + \text{OH-GDGT-1} \\ & + \text{OH-GDGT-2}]}{\Sigma[\text{OH-GDGT-0} \\ & + \text{OH-GDGT-1} + \text{OH-GDGT-2}] \\ & + \Sigma[\text{GDGT-0} + \text{GDGT-1} + \text{GDGT-2} \\ & + \text{GDGT-3} + \text{cren} + \text{cren}']} \times 100 \end{aligned} \quad (5)$$

The ring indices of hydroxylated tetraethers (RI-OH and RI-OH') quantify the degree of cyclisation, that is, the number of cyclopentane rings in the molecules. This number increases with temperature and decreases with salinity (Sinninghe Damsté et al., 2022). The RI-OH' is more sensitive in cold regions (Varma et al., 2024). The indices were calculated following Lü et al. (2015):

$$\begin{aligned} \text{RI-OH} = & \{[\text{OH-GDGT-1}] + 2 \\ & \times [\text{OH-GDGT-2}]\} / \{[\text{OH-GDGT-1}] \\ & + [\text{OH-GDGT-2}]\} \end{aligned} \quad (6)$$

$$\begin{aligned} \text{RI-OH}' = & \{[\text{OH-GDGT-1}] + 2 \\ & \times [\text{OH-GDGT-2}]\} / \Sigma[\text{OH-GDGTs}] \end{aligned} \quad (7)$$

3 Results

3.1 Porewater profiles of SO_4^{2-} , CH_4 , and Cl^-

Pockmarks across all sites show greater sulphate depletion, with a mean SO_4^{2-} concentration $1.5 \times$ lower than in non-pockmarks (1.93 ± 3.33 SD mM vs. 3.78 ± 3.72 SD mM, respectively, Fig. 2). Although SO_4^{2-} concentrations span similar value ranges in pockmarks and non-pockmarks (0.03–10.33 mM vs. 0.07–10.73 mM, respectively), their median values differ substantially by a factor of ~ 5 (0.39 vs. 1.99 mM, respectively). Pockmarks also show SO_4^{2-} depletion occurring closer to the surface, meaning the depth at which SO_4^{2-} first drops below 1 mM (at 17.3 ± 5.9 cm in pockmark cores compared with 36.3 ± 23.5 cm in reference cores) and 0.5 mM (17.3 ± 5.9 cm in pockmark cores compared with 49.7 ± 27.8 cm in reference cores) is 2 and 3 \times shallower, respectively. Pockmarks show mean CH_4 concentrations 2.3-fold higher than at reference sites (3.1 ± 2.6 mM vs. 1.3 ± 1.4 mM, mean \pm SD; Fig. 2). Median CH_4 concentrations were also higher in pockmark-cores (2.24 vs. 1.44 mM; on average 3.11 ± 2.56 vs. 1.34 ± 1.38 mM), reflecting the influence of particularly high CH_4 concentrations in selected pockmark horizons (ranging 0–11.89 mM) compared with non-pockmark ones (0–4.56 mM). MET4 exhibits the most extreme values across the examined sites and the greatest differences between pockmark and reference cores; CH_4 reached the highest values in the pockmark core, whereas the reference core remained close to CH_4 -free. By contrast, MET3 shows the least differentiation between pockmark and reference cores and has lower overall methane concentrations.

Sulphate and CH_4 show clear, opposing depth trends across all four study locations, except at non-pockmark S/MET4, where CH_4 is absent, and sulphate is high throughout the profile (Fig. 2). SO_4^{2-} is initially high in surface sediments and declines with depth, whereas CH_4 shows the opposite pattern. For the purpose of this study, the SMI is defined as the layer within the sediment at which the porewater concentrations of SO_4^{2-} and CH_4 are equal. At this interface, AOM couples SO_4^{2-} reduction to CH_4 oxidation, consuming most of the CH_4 and SO_4^{2-} and producing low concentrations of both. The depth of SMI, as well as the differences between pockmark and reference sites, vary by location, with SMI in pockmarks located closer to the sediment surface (Fig. 2). In pockmark sediments, the SMI was located 5–15 cm below the seafloor, whereas in non-pockmark sediments it was 10–50 cm below the seafloor. At MET1-BH and MET3, the SMI in the pockmarks was shallower than at the reference stations; at MET1-MP, the SMI in the pockmark was similarly shallow to that at the reference site; at MET4, no SMI was detected within the sampled interval at the non-pockmark site, while the pockmark exhibited a shallow SMI.

Chloride porewater profiles differed among the investigated sites, with generally lower concentrations in pockmark cores (151.39 ± 31.13 mM) than in reference cores (174.84 ± 18.43 mM) (Fig. 2).

The strongest contrast between the pockmark and reference cores is evident at MET4 (Fig. 2). This contrast reflects a pronounced downcore Cl^- depletion in the P/MET4 pockmark core (from 195.40 mM at the surface to 117.97–126.66 mM below 50 cm depth), compared with the reference core, which shows consistently higher and steady Cl^- concentrations (170.94–205.33 mM). This pattern indicates freshwater enrichment within the P/MET4 pockmark core relative to the adjacent reference core. However, the lowest concentrations occur in the MET1-MP pockmark core, where Cl^- decreases steadily with depth (from 167.50 mM at the surface to 80.76 mM at the bottom). Whereas Cl^- concentrations also decrease with depth in the reference core of MET1-MP (ranging 130.86–180.71 mM), they remain higher than in the MET1-MP pockmark core (Fig. 2). In the MET1-BH pockmark core, Cl^- concentrations are lower than in the reference core throughout the sediment profile, but the pattern is irregular (a dip to 131.65 mM at 20 cm and a recovery to ~ 147 –158 mM below). In the MET1-BH reference core, Cl^- concentrations are higher and more variable (155.49–192.89 mM). At MET3, the pockmark and reference cores are largely similar across the depth profile and remain among the highest Cl^- levels in the dataset (134.87–196.98 mM, median 189.44 ± 18.24 vs. 174.67 – 197.88 mM, median 184.44 ± 6.9 , respectively). The main difference appears in the deepest P/MET3 pockmark sample, where the Cl^- concentration drops (134.87 mM at 85 cm), whereas the reference core remains constant (Fig. 2).

3.2 LOI

LOI-derived estimates of organic matter are sensitive to ignition conditions and sediment composition. Because mass loss at 550 °C may include contributions from sediment mineralogy, including inorganic carbon-bearing minerals, LOI-based values provide a screening-level estimate of TOC rather than an exact measurement of organic matter content. To assess whether LOI captured the main downcore stratigraphic trends in organic carbon, LOI profiles were compared with directly measured TOC in two representative cores: the MET1-MP pockmark core and the MET3 reference core (Fig. S2).

Consistent with the regional relationship between TOC and LOI reported in the Gdańsk Basin by Łukawska-Matuszewska et al. (2014) across all paired measurements, TOC and LOI in the pockmark core P/MET1-MP and the reference core S/MET3 are significantly correlated ($r = 0.65$, $p < 0.005$), and linear regression explains 43 % of the variability in TOC ($R^2 = 0.43$; $\text{TOC} = 0.612 + 0.282 \text{ LOI}$). The positive correlation between LOI and TOC supports using LOI as a proxy for organic matter variability. In both cores, intervals of increased LOI predominantly coincide with higher measured TOC, demonstrating that LOI reliably reflects variations in organic matter content, despite differences (Fig. S2).

In the MET1-MP pockmark core, both LOI and measured TOC are relatively elevated in the upper to middle part of the core and generally decrease below ~ 45 – 55 cm depth (Fig. S2). This indicates a downcore decline in bulk organic matter content below the mid-core interval. In the S/MET3 reference core, measured TOC is highest in the shallowest interval, decreases through the upper-middle section of the core, and subsequently increases in deeper intervals, while LOI follows a comparable vertical pattern (Fig. S2). Therefore, LOI is used below as a qualitative, high-resolution proxy for bulk organic matter trends in the studied cores, providing a sedimentary and geochemical context for the GDGT and microbial distributions.

LOI values show site-specific and downcore variability, with varying degrees of contrast between pockmark and reference cores, indicating differences in bulk organic matter content and relative enrichment in pockmark cores, especially pronounced in MET1-BH (Fig. 3). In the MET1 area, the same reference core was used for comparison with the MET1-MP and MET1-BH pockmarks. LOI values were elevated in pockmark cores compared with reference cores, particularly in MET1-BH and MET1-MP, with LOI values on average approximately 2.2-fold higher in the MET1-BH pockmark core and 1.3-fold higher in the MET1-MP pockmark core relative to the shared MET1 reference core. The strongest enrichment occurs at MET1-BH, where pockmark LOI values are about 1.9–3.0 times higher than the corresponding reference values. In contrast, pockmark P/MET3 shows only a weak average difference of ~ 1.1 -fold, with

depth-wise ratios ranging from 0.7 to 1.3, indicating that LOI values at MET3 are broadly overlapping between pockmark and reference cores.

At MET4, pockmark LOI values were on average ca. 1.4-fold higher than in the reference core, with the relative difference elevated in the uppermost part of the profile (10–15 cm), decreasing below that section, and increasing again in the middle part of the profile, reaching approximately 2.1-fold in the deepest interval of the profile, where the reference core shows low LOI values of ~ 4 % (Fig. 3). The LOI results, used as a proxy for organic matter content, indicate that organic matter accumulation is site-specific and should not be generalised across all pockmarks.

3.3 iGDGTs in pockmark and non-pockmark marine surface sediments

The abundance and distribution of iGDGTs (GDGT-0 to GDGT-3, crenarchaeol, and its isomer) were analysed in pockmark core sediments and in surrounding non-pockmark reference core sediments (Fig. 4). All targeted iGDGTs were detected in both settings.

Unless stated otherwise, concentration values are reported as ranges, followed by the median and the mean \pm standard deviation (SD). Summed iGDGT concentrations (Σ iGDGTs) span 0.02–58.85 $\mu\text{g g}^{-1}$ sediment across all samples, with values generally higher and more variable in pockmark sediment cores (0.92–58.85 $\mu\text{g g}^{-1}$ sediment; 5.10 $\mu\text{g g}^{-1}$; 10.58 \pm 13.08 $\mu\text{g g}^{-1}$) than in reference sediment cores (0.02–16.81 $\mu\text{g g}^{-1}$ sediment; 2.59 $\mu\text{g g}^{-1}$; 3.73 \pm 3.41 $\mu\text{g g}^{-1}$), that is, approximately twice the median and three times the mean. Spatially, the highest Σ iGDGT concentrations occur at sites in the Gdańsk Deep (MET3, MET4), whereas lower concentrations are generally observed in the MET1 area (Fig. 4). With depth, Σ iGDGTs commonly show shallow to mid-depth maxima, particularly between approximately 15 and 45 cm b.s.f., followed by downcore depletion. Excluding the anomalously low values in the S/MET4 reference core, Σ iGDGTs concentrations typically decline by a factor of ~ 2.6 to ~ 64 , although the fold decrease is much larger where the deepest reference intervals approach near-zero values in S/MET4.

Crenarchaeol (cren) is the dominant iGDGT in both pockmark cores (mean fractional abundance of 0.53 \pm 0.03 SD) and reference cores (0.55 \pm 0.02 SD) (Fig. 5). GDGT-0 is the second most abundant in pockmark and reference cores (0.43 \pm 0.03 SD; 0.41 \pm 0.02 SD, respectively) (Fig. 5). Together, crenarchaeol and GDGT-0 account for ~ 96 % of the total iGDGT pool in both pockmark and reference cores, indicating broadly similar iGDGT distributions between pockmarks and references. Consistently, GDGT-0 covaries very strongly with crenarchaeol ($r = 0.996$, $p < 0.001$).

The remaining iGDGTs, GDGT-1 to GDGT-3, occur only in minor proportions and at much lower concentrations (Fig. 5). Across the analysed depth intervals from 0–5 to 90–

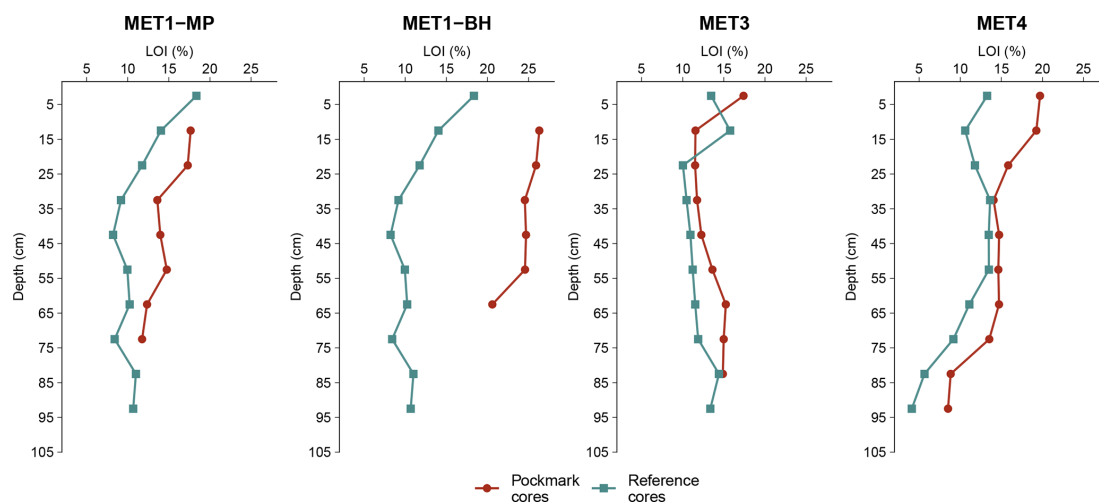


Figure 3. Downcore variation of loss-on-ignition (LOI%) in sediment cores collected from the Gulf of Gdańsk (MET1-MP, MET1-BH) and the Gdańsk Deep (MET3, MET4), south-eastern Baltic Sea. LOI values are plotted against depth bsf and serve as a qualitative, screening-level proxy for variability in bulk organic matter. Pockmark sediments are compared with adjacent reference (non-pockmark) sediment cores at each site; for the MET1-MP and MET1-BH pockmarks, the same reference core is used. LOI values are elevated in the pockmark cores at MET1-MP, MET1-BH, and MET4, with the strongest enrichment observed at MET1-BH. By contrast, MET3 shows values that are approximately overlapping between the pockmark and reference sediment cores. At MET4, both cores show a pronounced downcore decrease in LOI, particularly in the reference core, where values decline to ca. 4% in the deepest part of the profile.

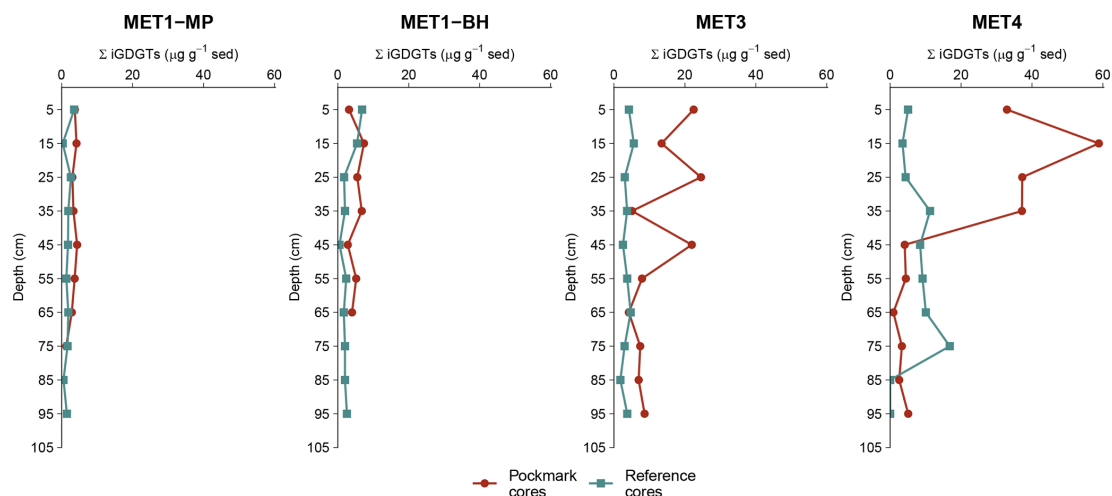


Figure 4. Downcore profiles of summed isoprenoidal glycerol dialkyl glycerol tetraethers (Σ iGDGTs; $\mu\text{g g}^{-1}$ dry sediment) for sediment cores from four sites in the south-eastern Baltic Sea: MET1-MP and MET1-BH (Gulf of Gdańsk), and MET3 and MET4 (Gdańsk Deep). Concentrations are plotted as a function of depth bsf, showing a general downcore decrease. Σ iGDGTs exhibit elevated concentrations in pockmark sediment cores relative to adjacent reference sediment cores, with the most pronounced enrichment observed at the Gdańsk Deep sites (MET3, MET4), where elevated near-surface values are followed by a downcore decrease. Error bars are not shown because each point represents a single sediment horizon analysed once (see Sect. 2.5).

95 cm b.s.f., GDGT-1, GDGT-2, and GDGT-3 show a highly consistent pattern of relative abundance. In 74 of 75 samples, the order is GDGT-1 > GDGT-2 > GDGT-3, and GDGT-2 is not the dominant compound in any sample. The only exception is sample P/MET4/3, where the order is GDGT-1 > GDGT-3 > GDGT-2.

Concentration profiles of the individual iGDGTs (Fig. S4) generally follow similar downcore patterns, except for isolated concentration maxima of GDGT-1 in P/MET1-BH/6 and GDGT-3 in P/MET4/3, minor changes in the crenarchaeol isomer (cren/) at MET1-MP and MET1-BH, and even smaller differences at MET3 and MET4. GDGT-1, GDGT-2, and GDGT-3 also show strong covariation with crenarchaeol

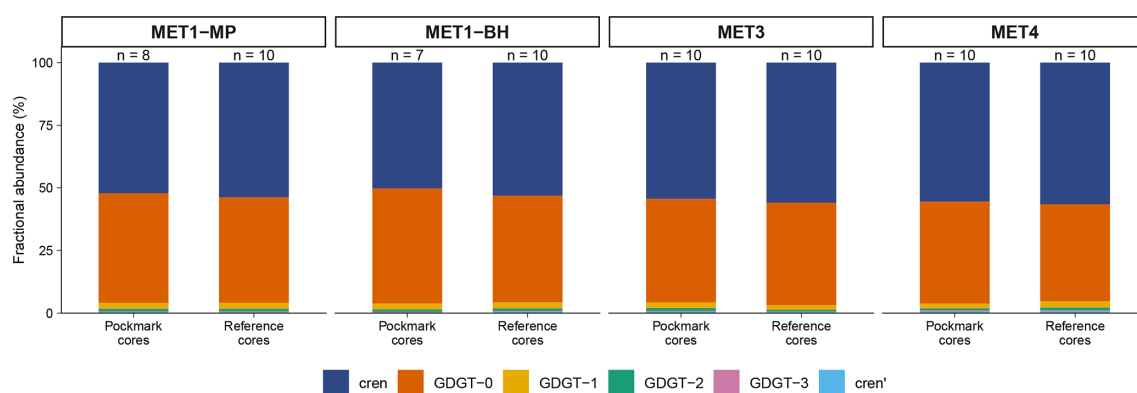


Figure 5. Mean fractional abundances of iGDGTs in pockmark and reference cores at sites MET1-MP, MET1-BH, MET3, and MET4 in the south-eastern Baltic Sea. Stacked bars show mean fractional abundances of iGDGTs (GDGT-0–3, crenarchaeol, and cren'), averaged by site and core type; *n* indicates the number of horizons (samples). The upper panel shows the full scale (0%–100%). Crenarchaeol and GDGT-0 dominate across all sites, whereas GDGT-1–3 and cren' constitute minor fractions.

($r = 0.988, 0.954, 0.951, p < 0.001$). Across all iGDGT pairs, correlations are consistently strong ($r = 0.847–0.996, p < 0.001$), indicating that the individual iGDGTs vary largely in concert rather than exhibiting compound-specific enrichments.

The mean \pm SD values for the indices are reported in Table 1. The GDGT-0/cren ratio is moderate and broadly comparable between pockmark and reference cores, ranging from 0.65 to 0.99 in pockmark cores and from 0.63 to 0.91 in reference cores (downcore variability shown in Fig. S3). No consistent downcore trend is observed across all cores; where changes occur, they are site-specific and modest relative to the overlap between pockmark and reference cores. The GDGT-2/cren ratio is consistently low (0.01–0.04), and MI values remain low, ranging from 0.04 to 0.09 in pockmarks and from 0.03 to 0.07 in references. The BIT index values are generally low, ranging from 0.008 to 0.14 in pockmarks and from 0.034 to 0.47 (to 0.17 without two S/MET4/9–10 outliers) in references, with the slightly higher values in reference cores.

3.4 OH-GDGTs in pockmark and non-pockmark sediments

The abundance and distribution of hydroxylated GDGTs (OH-GDGT-0 to -2) in pockmark and reference cores broadly mirror those of iGDGTs, with strong positive cross-correlations ($r = 0.840–0.992, p < 0.001$) and the tightest coupling with GDGT-0 (Σ OH-GDGTs: $r = 0.992, p < 0.001$) and crenarchaeol ($r = 0.983, p < 0.01$). All targeted OH-GDGTs (OH-GDGT-0 to -2) were detected in both settings.

Summed OH-GDGT concentrations (Σ OH-GDGTs) ranged from 0.00 to $6.30 \mu\text{g g}^{-1}$ sediment across all samples, with values generally higher in pockmark sediment cores ($0.06–6.30 \mu\text{g g}^{-1}$ sediment; $0.43 \mu\text{g g}^{-1}$ sediment; $1.02 \pm 1.36 \mu\text{g g}^{-1}$ sediment) than in reference sediment

cores ($0.00–1.75 \mu\text{g g}^{-1}$ sediment; $0.21 \mu\text{g g}^{-1}$ sediment; $0.31 \pm 0.32 \mu\text{g g}^{-1}$ sediment) (Fig. 6). Σ OH-GDGTs are therefore, on average, approximately three times higher and, at the median, about twice as high in pockmarks as in references. Spatially, the highest Σ OH-GDGTs concentrations occur at MET4, intermediate values at MET3, and lower values in the MET1 area, broadly mirroring the spatial pattern observed for Σ iGDGTs. With depth, Σ OH-GDGTs commonly show shallow to mid-depth maxima, typically between 15 and 45 cm b.s.f., followed by downcore depletion (Fig. 6). This decrease is particularly pronounced at MET4, especially in P/MET4, where Σ iGDGTs declined from 6.30 to $0.06 \mu\text{g g}^{-1}$ sediment.

Across all cores, OH-GDGTs are dominated by OH-GDGT-0 in both pockmark and reference cores (Fig. 7, average fractional abundances of 0.83 ± 0.02 SD and 0.82 ± 0.03 SD, respectively). OH-GDGT-1 and OH-GDGT-2 are consistently minor components (Fig. 7). Overall, OH-GDGT distributions are broadly similar between pockmark and reference cores (Fig. S5), and most variability is evident in downcore concentration profiles, which typically decline by a factor of ~ 1.2 to ~ 7.8 , with most cores showing an average decrease by a factor of ~ 3 (except for S/MET4, which declines to zero at the base). Across all OH-GDGT pairs (OH-0, OH-1, OH-2), correlations are consistently very strong ($r = 0.975–0.992, p < 0.01$).

OH-GDGT% and RI-OH show only minor differences between pockmark and reference cores (Table 1). OH-GDGT% values are slightly higher in pockmarks (6.4–9.9) than in references (6.2–9.4). RI-OH is identical between settings (1.1–1.3 in pockmarks; 1.1–1.3 in references), whereas RI-OH/cren is modestly higher in references (0.16–0.36) than in pockmarks (0.16–0.25). Overall, variability in OH-GDGTs is mainly reflected in absolute abundances, while OH-GDGT distribution and indices are broadly comparable between pockmark and reference cores.

Table 1. Mean GDGT-based indices for pockmark (P) and reference (S) sediment cores at MET1 (MP, BH), MET3, and MET4. Values are reported as mean \pm sample standard deviation, rounded to a maximum of two significant figures. Metrics include OH-GDGT%, hydroxylated GDGT ring indices (RI-OH, RI-OH'), the Branched and Isoprenoid tetraether index (BIT), the Methane Index (MI), and diagnostic ratios (GDGT-0 / cren, GDGT-2 / cren). RI-OH shows minimal variation across sites and between pockmark and reference cores (~ 1.1 – 1.2), indicating comparable OH-GDGT cyclisation patterns. OH-GDGT% is moderately elevated at MET1 relative to MET3–MET4, with minimal within-site variation. MI values remain consistently low (0.05–0.07). GDGT-0 / cren ratios are consistently slightly elevated in pockmark cores relative to paired references, whereas GDGT-2 / cren remains uniformly low (0.01–0.02), indicating that pockmark influence primarily affects GDGT-0 abundance rather than higher-cyclised GDGTs. Downcore variability of MI, BIT, RI-OH, RI-OH', and GDGT-0 / cren is shown (Fig. S3).

Sediment core	OH-GDGT%	RI-OH	RI-OH'	BIT	MI	GDGT-0 / cren	GDGT-2 / cren
P/MET1-MP	9.0 \pm 0.4	1.2 \pm 0.03	0.19 \pm 0.02	0.12 \pm 0.01	0.065 \pm 0.003	0.84 \pm 0.02	0.019 \pm 0.001
P/MET1-BH	9.3 \pm 0.4	1.2 \pm 0.04	0.19 \pm 0.02	0.09 \pm 0.01	0.066 \pm 0.003	0.92 \pm 0.04	0.019 \pm 0.002
P/MET3	7.9 \pm 0.9	1.2 \pm 0.02	0.21 \pm 0.03	0.05 \pm 0.02	0.064 \pm 0.008	0.76 \pm 0.11	0.021 \pm 0.004
P/MET4	7.8 \pm 1.3	1.1 \pm 0.02	0.19 \pm 0.02	0.03 \pm 0.02	0.054 \pm 0.016	0.74 \pm 0.08	0.014 \pm 0.003
S/MET1-MP	8.1 \pm 0.8	1.2 \pm 0.04	0.25 \pm 0.04	0.14 \pm 0.03	0.066 \pm 0.002	0.79 \pm 0.05	0.019 \pm 0.001
S/MET1-BH	8.1 \pm 0.9	1.2 \pm 0.02	0.23 \pm 0.03	0.12 \pm 0.02	0.066 \pm 0.003	0.80 \pm 0.06	0.019 \pm 0.001
S/MET3	7.0 \pm 0.6	1.2 \pm 0.03	0.19 \pm 0.02	0.07 \pm 0.01	0.047 \pm 0.003	0.73 \pm 0.07	0.013 \pm 0.001
S/MET4	7.2 \pm 0.9	1.2 \pm 0.06	0.21 \pm 0.07	0.13 \pm 0.16	0.065 \pm 0.036	0.69 \pm 0.03	0.019 \pm 0.013

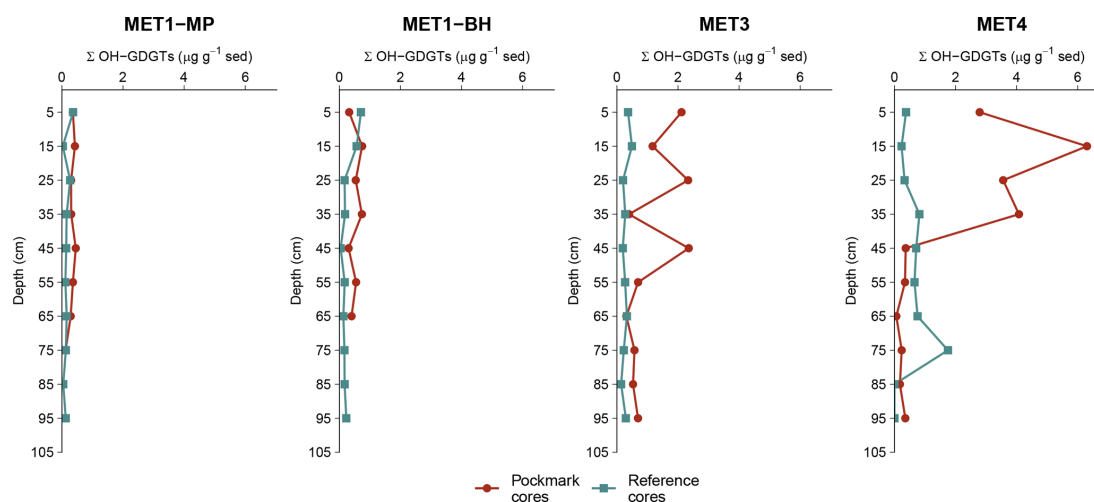


Figure 6. Downcore profiles of summed hydroxylated glycerol dialkyl glycerol tetraethers (Σ OH-GDGTs; $\mu\text{g g}^{-1}$ dry sediment) for sediment cores from four sites in the south-eastern Baltic Sea: MET1-MP and MET1-BH (Gulf of Gdańsk) and MET3 and MET4 (Gdańsk Deep). Concentrations are plotted against depth (downcore increase; cm). Σ OH-GDGT concentrations follow the pattern of iGDGTs, showing strong positive cross-correlations and the highest coupling with GDGT-0 and crenarchaeol (see Sect. 3.2). In the Gulf of Gdańsk (MET1-MP, MET1-BH), Σ OH-GDGTs show lower overall abundances than iGDGTs but remain elevated in pockmark intervals relative to reference sediments.

3.5 Abundance and composition of archaea

Archaeal community composition differs between pockmark and reference sediments (Fig. 8). However, at the class level, most samples are dominated by Nanoarchaeia (Fig. 8a). Additional major contributions, at varying proportions, include Thermoplasmata, Methanosarcinia, Thermococci, Bathyarchaeia, Lokiarchaeia, and Methanomicrobia (Fig. 8a). Pockmark samples generally contain higher proportions of methane-cycling archaeal groups, particularly Methanosarcinia and Methanomicrobia, whereas reference cores more commonly show elevated contributions

of Thermoplasmata, Bathyarchaeia, and Lokiarchaeia (Fig. 8a). The general depth trend shows Nanoarchaeia dominating shallower horizons, uniformly across reference and pockmark cores. Nanoarchaeia dominate the archaeal community in pockmarks, even in deeper sediment horizons, particularly at P/MET1-BH and P/MET1-MP. Vertical stratification is less consistent and more site-specific in pockmark cores than in reference cores, but the relative abundance of Methanosarcinia, Thermococci, and Bathyarchaeia increases downcore. Methanomicrobia also show a pockmark-associated pattern, with higher mean relative abundance in

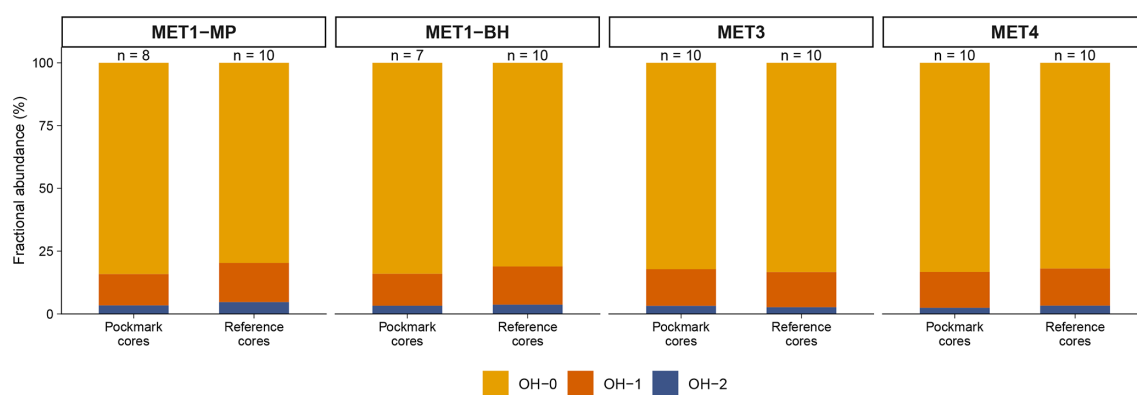


Figure 7. Mean OH-GDGT fractional abundances in pockmark versus reference cores at sites MET1-MP, MET1-BH, MET3, and MET4 in the south-eastern Baltic Sea. Stacked bars show mean fractional abundances of OH-0, OH-1 and OH-2, averaged by site and core type (pockmarks and references); n denotes the number of horizons (samples). OH-0 dominates across all sites, with OH-1 contributing a smaller yet consistent fraction and OH-2 occurring at low abundance.

pockmarks than in references ($2.6 \pm 1.8\%$ vs. $0.6 \pm 1.0\%$, respectively), indicating additional methanogen-affiliated archaeal populations beyond Methanosarcinia (Fig. 8a). In reference cores, in deeper horizons, the community composition shifts towards a higher relative abundance of Thermoplasmata, Bathyarchaeia, Lokiarchaeia, and Deep Sea Euryarchaeotic Group (DSEG, currently within Thermoplasmata; Rinke et al., 2021), suggesting a greater contribution from uncultivated anaerobic sedimentary archaeal lineages with depth. Across all samples, these classes were more abundant in reference than in pockmark cores, with mean relative abundances of $20.5 \pm 13.6\%$ vs. $9.4 \pm 5.2\%$ for Thermoplasmata, $14.8 \pm 19.5\%$ vs. $5.2 \pm 5.9\%$ for Bathyarchaeia, $5.6 \pm 2.4\%$ vs. $3.5 \pm 2.6\%$ for Lokiarchaeia, and $3.0 \pm 1.7\%$ vs. $2.0 \pm 1.8\%$ for DSEG.

Archaeoglobi were more abundant in reference sediments, averaging $1.7 \pm 1.9\%$ and $0.4 \pm 0.6\%$, respectively, particularly in mid-depth horizons, where they may indicate a sulphur-cycling anaerobic archaeal community (Fig. 8a). Other low-abundance classes, including Micrarchaeia, Iainarchaeia, Altiarchaeia and Heimdallarchaeia, formed part of the archaeal rare biosphere and exhibited localised enrichment in selected horizons. ANME-1 was detected only at trace relative abundance.

Nitrososphaeria were detected in both pockmark and reference cores, with taxonomic profiling revealing that this class is dominated almost exclusively by Nitrosopumilaceae (Fig. 8e, Fig. S6) and, at the genus level, primarily by *Ca. Nitrosopumilus* (Fig. S7a, b). Nitrosopumilaceae showed higher relative abundance in reference cores ($14.0 \pm 8.8\%$) than in pockmark cores ($8.8 \pm 3.7\%$), with maxima in deeper reference sediment strata. *Ca. Nitrosopumilus* was more abundant in reference cores, particularly in S/MET3/10, S/MET1-MP/10, and S/MET1-BH/10 (Fig. S7a, b). These distributional trends indicate that Nitrosopumilaceae-affiliated AOA are a more signif-

icant component of the biogeochemical nitrogen-cycling community in non-pockmark and deeper sediment horizons, whereas selected pockmark layers are comparatively enriched in archaeal taxa implicated in CH_4 cycling. This indicates that the distinction between pockmark and reference sediments is largely reflected in shifts in the relative abundance of CH_4 -cycling, heterotrophic/fermentative, and ammonia-oxidising archaeal groups.

Hierarchical analysis at the class level showed four distinct clusters (Fig. 8b), with partial clustering of pockmark and reference samples and overlap between the pockmark and reference cores. Cluster 1 comprises the pockmark samples; Cluster 2 combines reference and pockmark samples; Cluster 3 groups mainly reference samples; and Cluster 4 comprises two S/MET1-BH reference samples and the P/MET4/10 sample (outliers). This pattern is consistent with the MDS ordination. The PERMANOVA test (Fig. 8c) indicates that the difference between pockmark and reference archaeal communities is statistically significant ($p = 0.003$). Multivariate analysis using MDS clearly shows clustering of samples into two categories – pockmarks vs. references (Fig. 8c). However, some differences are noticeable: pockmark samples are more tightly clustered, whereas reference samples are slightly more dispersed. Based on the above analyses, it can be assumed that the pockmark cores differ significantly in their archaeal composition from the adjacent reference cores. Additionally, PCA analysis indicates the groups that may have the greatest impact on sample differentiation (Fig. 8d). For pockmarks, the greatest impact on sample variability is as follows: Hadarchaeia > Methanobacteria > Methanocellia > Halobacteria. In the reference samples, the order is Methanocellia > ANME-1 > Methanobacteria > Hadarchaeia. In both pockmark and reference cores, the same groups contribute most to sample variability, although the proportions of these contributions differ; therefore, the compositions must differ.

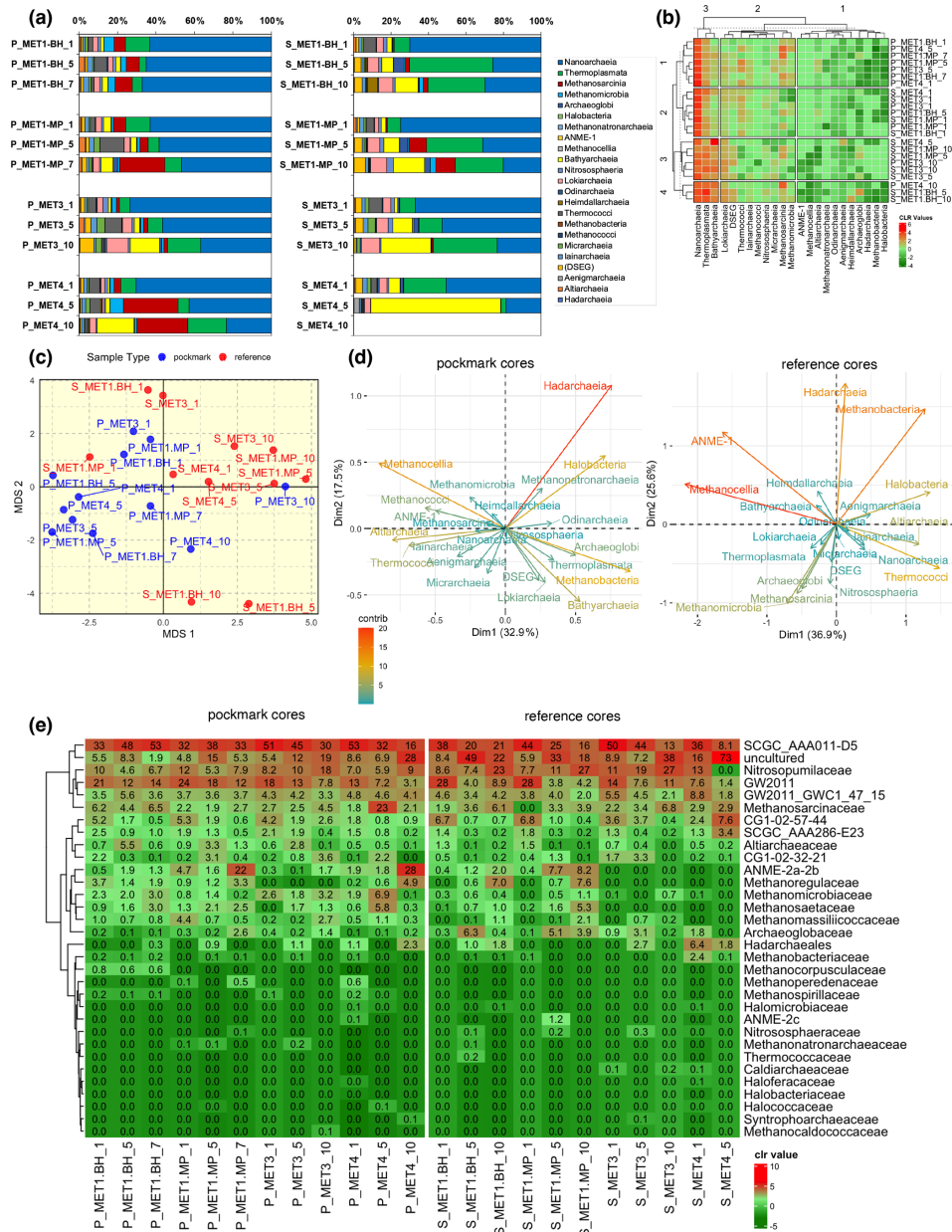


Figure 8. Archaeal community composition and multivariate structure in pockmark and reference sediment cores from the south-eastern Baltic Sea. **(a)** Class-level relative abundance profiles (stacked bars) of archaeal communities in pockmark (P) and reference (S) sediment samples from MET1-BH, MET1-MP, MET3, and MET4. Bars show the proportional contribution of archaeal classes in each sample; sample suffixes indicate depth horizons (as explained in Sect. 2.2). **(b)** Class-level heatmap of centred log-ratio (CLR)-transformed relative abundances, with hierarchical clustering (dendrograms) of samples and archaeal classes, showing covariation among classes and samples, where red indicates higher relative enrichment and green indicates lower relative enrichment. **(c)** Multidimensional scaling (MDS) ordination of archaeal community composition shows partial separation between pockmark and reference samples (PERMANOVA, $p = 0.003$). MDS shows significant separation (PERMANOVA, $p = 0.003$), with reference samples more dispersed and pockmark samples more tightly grouped. Taxa driving within-group variability differ between habitats: Hadarchaeia and Halobacteria dominate the pockmark ordination, whereas Methanobacteria, ANME and Hadarchaeia drive the reference ordination. **(d)** Ordination biplot showing the archaeal classes that contribute most strongly to community variation in pockmark and reference samples, respectively. Nanoarchaeia dominate across all sites. Pockmark horizons show elevated Methanosarcinia (MET1-MP, MET4), whereas reference horizons show stronger contributions from Thermoplasmata and/or Bathyarchaeia. Hierarchical clustering reveals partial intermixing of pockmark and reference samples, indicating that community structure reflects both habitat type and site-specific variability. **(e)** Family-level heatmap of archaeal relative abundance (CLR-transformed community structure), showing taxonomic groups not visible at the class level, i.e., ANME-2a-2b.

Because several archaeal groups discussed in relation to methane cycling and ammonia oxidation are not resolved at the class level, the family-level heatmap is presented to clarify the distribution of key taxa (Fig. 8e). Additional figures in the supplementary material show extended family-level relative abundance profiles (Fig. S6), the genus-level heatmap with extended genus-level relative abundance profiles (Fig. S7a, b), and profiles revealing the relative abundances of methanogenic (Fig. S8) and methanotrophic (Fig. S9) archaeal groups.

At the family level, a few groups dominate both pockmark and reference cores, albeit in different proportions: SCGC_AAA011-D5, uncultured lineages, GW2011, and Nitrosopumilaceae (Fig. 8e). However, there are some site- and horizon-specific distinctions. Pockmark cores are characterised by a strong, localised enrichment of methane-cycling archaea, particularly ANME-2a-2b group (mean relative abundance of $5.5 \pm 9.3\%$ vs. $1.8 \pm 3.1\%$), Methanosarcinaceae ($5.0 \pm 6.0\%$ vs. $3.4 \pm 1.9\%$), Methanomicrobiaceae ($2.2 \pm 1.8\%$ vs. $0.3 \pm 0.4\%$), and Methanosaetaceae ($1.8 \pm 1.5\%$ vs. $0.8 \pm 1.6\%$). These taxa show vertical heterogeneity, with relative abundances peaking at the middle and bottom of the profiles, i.e., ANME-2a-2b group in the deeper parts of the pockmark cores (P/MET1-MP/7, P/MET4/10; Fig. 8e; Fig. S6), as well as Methanosarcinaceae (P/MET4/5; Fig. 8e; Fig. S6) and Methanomicrobiaceae (P/MET4/5; Fig. 8e; Fig. S6). Reference cores, by contrast, show a stronger contribution from Nitrosopumilaceae ($14.0 \pm 8.8\%$ vs. $8.8 \pm 3.7\%$), Archaeoglobaceae ($2.0 \pm 2.3\%$ vs. $0.5 \pm 0.7\%$), Hadarchaeales ($1.3 \pm 2.0\%$ vs. $0.5 \pm 0.7\%$), and uncultured lineages ($25.3 \pm 21.1\%$ vs. $10.1 \pm 7.4\%$) (Fig. 8e; Fig. S6), which are characterised by variable depth-related trends.

At the genus level, both pockmark and reference cores are dominated by AR15, *Ca. Nitrosopumilus*, Methanosarcina, and AR20 (Fig. S7). However, the archaeal community in pockmark cores shows a higher relative contribution of methanotrophic taxa than in reference cores, i.e., ANME-3 (minor component; $0.7 \pm 1.0\%$ vs. $0.1 \pm 0.4\%$), particularly in cores P/MET1-BH and P/MET4, and ANME-2b ($7.5 \pm 12.3\%$ vs. $1.9 \pm 4.1\%$), particularly in the upper and lower parts of the profiles P/MET1-MP and P/MET4; as well as enrichment of methanogens, particularly at mid-depth in P/MET4: Methanosarcina (29.3%), Methanosaeta (8.2%), and Methanogenium (5.9%). In contrast, reference cores show a stronger representation of *Ca. Nitrosopumilus* ($34.1 \pm 17.7\%$ vs. $22.3 \pm 7.4\%$), particularly at mid-depth in S/MET3, as well as AR20 ($7.5 \pm 6.1\%$ vs. $2.4 \pm 1.8\%$) and Methanoregula ($3.3 \pm 6.1\%$ vs. $2.8 \pm 3.5\%$), particularly at the bottom of the S/MET1-BH profile.

The methanogenic and methanotrophic groups are not restricted to pockmarks; in the reference cores, their relative abundances are lower, yet they remain common. The summed relative abundance of methanotrophic archaeal groups is approximately 4-fold higher in pockmark cores

than in adjacent reference cores, averaging $8.3 \pm 12.2\%$ and $2.0 \pm 4.1\%$, respectively. AOM-associated archaea, primarily ANME-2b and, to a lesser extent, ANME-3, are, however, enriched in selected pockmark horizons. Methanogenic archaea are abundant in both pockmark and reference cores, with a moderately higher average summed relative abundance in pockmarks ($18 \pm 11.4\%$) than in references ($14.0 \pm 11.4\%$). However, in pockmark cores, the diversity of methanogenic taxa, and to a lesser extent methanotrophic taxa, is higher (Figs S7, S8).

Archaeal read abundances were generally higher in pockmark cores than in reference cores, particularly at MET4, where abundances peak in the shallow horizon (Fig. S10). In pockmark cores, archaeal abundances typically peak in the upper to middle parts of the sampled profiles, except in P/MET1-BH, where the trend is reversed (Fig. S10). Similarly, in the reference cores, archaeal abundances peak in the upper to middle horizons, except in the S/MET1-BH core, where abundance increases with depth (Fig. S10).

3.6 Correlation network

To link GDGT patterns to probable biological sources, we combined iGDGT and OH-GDGT abundances with archaeal 16S rRNA relative abundances at the family level using correlation network analysis. This approach identified co-varying lipid–taxon modules that may indicate common sources, ecological niches, or interconnected processes rather than direct biosynthesis alone.

In pockmark sediments, the correlation network resolves three main archaeal communities that co-vary (Fig. 9). The first community (red) comprises the full suite of measured GDGTs and is most strongly connected to several Nanoarchaeia lineages (GW2011, SCGC_AAA286_E23, CG1.02.57.44, SCGC_AAA011.D5), with additional links to Methanoperedenaceae. The second community is dominated by ammonia-oxidising Nitrosopumilaceae and clusters with Hadarchaeales. Within this module, Nitrosopumilaceae show the strongest positive associations with GDGT-0, the remaining iGDGTs, and OH-GDGTs. The same module contains ANME-2a-2b, Methanoregulaceae, and uncultured lineages that are strongly interconnected with one another but show comparatively weaker links to GDGTs. Archaeoglobaceae form a peripheral node and does not link to any GDGTs in pockmarks. The third community comprises methanogenic lineages, including Methanospirillaceae, Methanobacteriaceae, Methanosarcinaceae, Methanosaetaceae, Methanomicrobiaceae, Methanomassiliicoccaceae and CG1.02.32.21 (associated with the order Micrarchaeales). These are less directly linked to GDGTs but strongly interlinked with one another. This cluster also includes another representative of Nanoarchaeia (GW2011_GWC1_47_15).

In reference sediments, GDGT associations are more broadly distributed across archaeal groups, and the network exhibits higher modularity, with clearer separa-

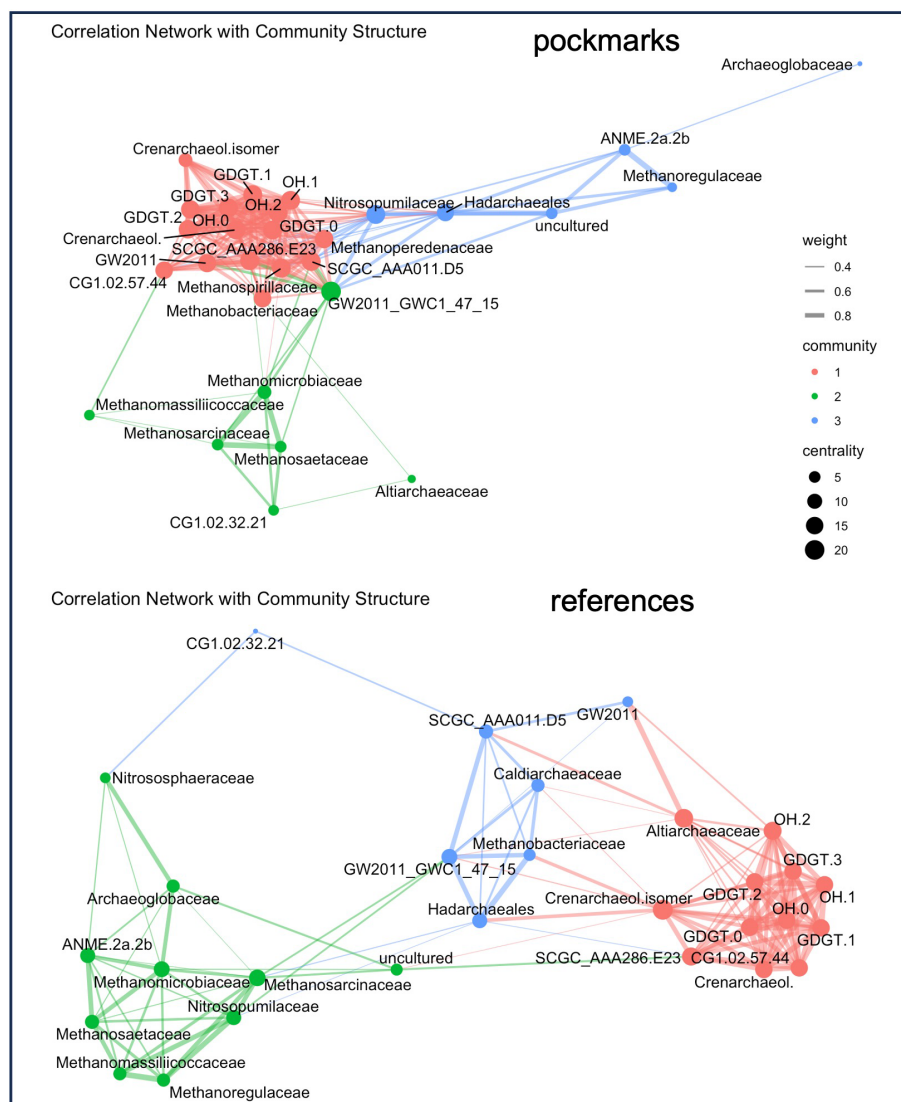


Figure 9. Correlation networks linking archaeal lipid biomarkers and community members in pockmark and reference (non-pockmark) sediments. Nodes represent lipid variables (GDGTs, OH-GDGTs) and archaeal taxa (family level). Edge thickness reflects correlation strength; node colour denotes modules/communities (1–3); node size reflects centrality (larger nodes indicate more central or highly connected features). Lipid variables form a tightly connected subnetwork (module 1; red), while additional modules comprise methane-cycling and other archaeal lineages. Module connectivity differs between pockmark and non-pockmark sites, indicating habitat-dependent coupling between biomarkers and archaeal taxa. Pockmark networks show tighter coupling between lipid biomarkers and methane-cycling lineages, whereas reference sediments display clearer module separation, with lipids and the archaeal community varying more independently.

tion among modules. A lipid cluster (crenarchaeol, cren/, GDGT-0-3, and OH-GDGTs) correlates with both ammonia oxidisers (Nitrosopumilaceae, Nitrososphaeraceae) and multiple methanogenic families (Methanosaetaceae, Methanosarcinaceae, Methanoregulaceae, Methanomicrobiaceae, Methanomassiliicoccaceae). Compared with pockmarks, methanogens show fewer direct links to the GDGT cluster and more to ANME-2a-2b. Archaeoglobaceae links to Nitrososphaeraceae and methanogens.

Overall, the pockmark network exhibits low modularity and relatively dense connectivity, indicating a closely cou-

pled archaeal community. At the same time, the strongest GDGT associations are observed with Nitrosopumilaceae, implying that AOA predominantly influence GDGT co-variation in pockmarks, whereas methanogens/ANME form more distinct sub-clusters characterised by weaker GDGT coupling.

4 Discussion

4.1 Archaeal community structure in methane-influenced pockmark sediment cores

The archaeal community structure and porewater profiles of CH₄ and SO₄²⁻ indicate that the investigated pockmarks are CH₄-influenced yet spatially heterogeneous sedimentary systems. At the microbial community level, pockmark cores are not characterised by a complete replacement of the archaeal groups inhabiting reference sediments, but rather by localised enrichment of CH₄-cycling lineages. This is most evident at lower taxonomic levels, where ANME-2b (genus-level distribution; Fig. S7a, b), ANME-2a-2b, Methanosarcinaceae, Methanosaetaceae, Methanomicrobiaceae (family-level distribution; Fig. 8e; Fig. S6), and other CH₄-associated taxa are enriched in selected pockmark horizons. Pockmark cores exhibit substantially higher methanogen diversity (11 genera detected) and a higher abundance of CH₄-cycling archaea (approximately 3-fold) than reference cores (6 genera) (Fig. S7a, b). Correspondingly, total iGDGT and OH-GDGT concentrations are approximately three times higher in pockmark cores than in reference cores (Figs. 4, 8). In the correlation network (Fig. 9), pockmarks represent a tightly coupled metabolic system in which various archaeal groups act in concert – likely CH₄-impacted – whereas at the reference sites these groups form less integrated sub-communities, with stronger representation of ammonia-oxidising *Ca. Nitrosopumilus* (Fig. S7a, b), heterotrophic Thermoplasmata associated with acidic, sulphur-rich environments (González-Toril et al., 2006), and organic matter-degrading Bathyarchaeia (Zhou et al., 2018). This suggests that in reference cores, microorganisms have more independent ecological roles, which could be explained by higher sulphate concentration and lower methane concentration (Fig. 2). On the other hand, the summed relative abundances of methanotrophic archaea are approximately 4-fold higher in pockmark cores than in reference cores, whereas methanogens are moderately more abundant in pockmark cores than in reference cores. This suggests that AOM-associated lineages are more closely linked to pockmark niches, whereas methanogenic taxa occupy broader anoxic sedimentary niches of the studied basin. The Gdańsk Basin is characterised by high organic matter loading resulting from eutrophication (Łukawska-Matuszewska et al., 2014), yet eutrophication and methanogenesis is widespread in the oxygen- and sulphate-depleted Baltic Sea (Schmale et al., 2010, with references therein; Carstensen et al., 2014; Lapham et al., 2024). However, the Baltic Sea exhibits considerable microbial diversity (Ininbergs et al., 2015), due to eutrophication and pollution, steep horizontal and vertical gradients in salinity and nutrient levels, the presence of freshwater and marine phyla, as well as autochthonous brackish populations.

4.2 Methanogenic archaea and depth-related community shifts

The absolute abundance of methanogens in pockmarks increases with sediment depth, except for the mid-depth of P/MET4, which harbours an excessive abundance of *Methanosarcina*. *Methanosarcina* predominates across all sediment horizons in both pockmark and reference cores (Fig. S8), likely owing to its metabolic versatility (Sowers et al., 1993; Galagan et al., 2002; Maeder et al., 2006), which confers competitive advantages under fluctuating environmental conditions (e.g., hydrostatic pressure governing freshened porewater seepage, seasonal thermocline dynamics, nutrient and organic matter availability, North Sea saline water inflow). The vertical distribution of methanogenic archaea varies with sediment depth (Fig. S8), whereas *Methanosarcina* and *Methanosaeta* predominantly populate the examined sediment horizons, except in the reference cores S/MET3 and S/MET4, which are dominated by *Methanosarcina*, and some of the bottom samples are dominated by *Methanoregula*. Both *Methanosarcina* and *Methanosaeta* drive acetoclastic methanogenesis (Conklin et al., 2006; Welte et al., 2014) and are favoured in sediments rich in labile organic matter (Li et al., 2022). Both are also major contributors to the GDGT-0 pool in estuarine sediments (De Rosa et al., 1977; Schouten et al., 2013; Bauersachs et al., 2015). At the same time, GDGT-0 is the second most abundant GDGT in the analysed samples after crenarchaeol (Fig. 5). The remaining major components of the methanogenic community that appear to alternate – sometimes with *Methanosaeta*, sometimes with SDB – are *Methanoregula* and *Methanogenium*, exhibiting a downcore shift.

Interestingly, a distinct dominance shift appears in the reference cores S/MET3 and S/MET4, where *Methanosaeta* is replaced by *Methanosarcina* (Fig. S8), which may indicate the onset of an environmental stressor, such as shifts in oxygen, ammonium, or organic matter concentrations that influence pH (De Vrieze, 2014). This shift coincides with a high relative abundance of *Ca. Nitrosopumilus*, *Ca. Aenigmarchaeum*, and Woesearchaeales (AR15, AR20) (Fig. S7a); however, the communities in the references S/MET3 and S/MET4 split into distinct groups, with surface AOA-DPANN-rich and subsurface different archaeal groups (Fig. 8b). In corresponding pockmark cores, *Methanosaeta* abundance declines remarkably in P/MET3 (especially in the uppermost sediment horizon) and in P/MET4 (especially in the lowermost horizon) and is replaced by diverse hydrogenotrophic genera, belonging to the Methanobacteria and Methanomicrobia class, including *Methanogenium*, *Methanospirillum*, *Methanomicrobium*, *Methanoculleus*, *Methanocorpusculum*, *Methanobrevibacter*, *Methanolinea*, *Methanoregula*, and SDB, which may indicate a seasonal shift towards hypoxic/anoxic conditions in bottom water and high organic matter degradation/supply.

This methanogenic community shift coincides with elevated CH₄ concentrations in the pockmarks P/MET3 and P/MET4 (Fig. 2). Adam-Beyer et al. (2025) directly link the presence and activity of Methanogenium in the incubation experiment on sediments collected in the South-Western Baltic Sea to phytoplankton blooms and a high supply of organic matter, resulting in organic matter degradation and oxygen depletion, which catalyse methanogenesis. In light of these findings, Kapustina et al. (2026) reported, at the time our samples were collected in October 2019, relatively high oxygen levels above the halocline (60–70 m) and hypoxic conditions below it (70–100 m), with permanent euxinia in the deep layers of the Gdańsk Deep (100 m and deeper). The contribution of hydrogenotrophic methanogens increases as the transition from freshened porewater-influenced pockmarks in the MET1 area of the Gulf of Gdańsk (mostly inferred from previous studies and discussed below in Sect. 4.3; Fig. S1) to marine conditions in the Gdańsk Deep is observed (i.e., higher sulphate concentrations, Fig. 2). The BIT index indicates a marine organic matter source with very low terrestrial input across both pockmark and reference cores; interestingly, the mean values increase along the Gulf of Gdańsk-Gdańsk Deep transect (Table 1; Fig. S3).

Pockmark core P/MET4 exhibits the highest total GDGT concentrations and the most pronounced individual GDGT peaks (Fig. 4; Fig. S4), whilst the second highest concentrations are observed in pockmark core P/MET3. The above-mentioned hydrogenotrophic Methanomicrobia are known to produce acyclic GDGTs (Bale et al., 2019; Zeng et al., 2022), and among Methanobacteria, genus *Methanobrevibacter* is an identified GDGT-0 producer (Bauersachs et al., 2015; Elling et al., 2017). However, in terms of relative abundance, *Methanosarcinia* and *Methanosaeta* in pockmarks are 1.25–1.65 times more abundant than hydrogenotrophic methanogens and 1–26.25 times more abundant than in references. Similar hydrogenotrophic communities have been documented in an inactive pockmark within the Hanko Basin, northern Baltic Sea (Purkamo et al., 2022). In this dataset, pockmark P/MET3 was inactive during the study period and showed no porewater freshening, whereas pockmark P/MET4 is characterised by weak seabed activity (Fig. S1, Table S1).

4.3 Porewater geochemistry, SMI development

Porewater profiles of CH₄ and SO₄²⁻ show stronger CH₄ accumulation and sharper SO₄²⁻ depletion, particularly at MET1-MP, MET1-BH, and MET4, indicating active or recent methane supply and shallow sulphate-methane interface (from 5 to ~15 cm bsf) where CH₄ and SO₄²⁻ gradients overlap (Fig. 2). In marine sediments, elevated seawater sulphate concentrations primarily limit microbial methane production to deeper sediment layers below the sulphatic zone (Jørgensen, 2021). However, in the studied pockmarks and reference sites of the MET1 area affected by porewater fresh-

ening, low sulphate concentrations below ca. 25 cm of sediment depth promote microbial methane production. Freshened groundwater seepage in the MET1 area, first reported by Idczak et al. (2020), Brodecka-Goluch et al. (2022), and Rzepa et al. (2026), significantly affects the microbial community by altering the chemical environment, leading to sulphate depletion in porewater and promoting methanogenesis throughout the entire sediment column rather than just in deeper layers. This was demonstrated by the dominance of Methanomicrobia during the freshwater outflow episode and of Nanoarchaea during the saltwater intrusion episode. Although in pockmark P/MET3 porewater freshening has not been observed and the Cl⁻ concentrations are similar to those of the reference core (Fig. 2), next to freshened porewater influence, sulphate depletion may be caused by high organic loading, where microbial demand for electron acceptors is high and sulphate is consumed rapidly. This typically occurs in the top metre of sediment below the seafloor in the Baltic Sea (Zinke et al., 2019).

Previously, it was suggested that freshened groundwater seepage dilutes the already low chloride and sulphate concentrations in the pockmarks MET1-BH and MET1-MP (Brodecka-Goluch et al., 2022; Idczak et al., 2020; Łukawska-Matuszewska and Dwornik, 2025). Chloride profiles in pockmarks MET1 and MET4 show lower Cl⁻ concentrations than adjacent reference cores (Fig. 2), suggesting that freshened porewater discharge may be diluting SO₄²⁻ (Fig. 2), thereby influencing both the depth and the archaeal community structure of the methane oxidation zone. Kurowski et al. (2024) analysed the MET1-BH pockmark and suggested that iron-dependent anaerobic oxidation of methane (Fe-AOM) serves as an alternative pathway when sulphate is limited in the MET1 area. The reduced SO₄²⁻ availability in porewaters of CH₄-rich Baltic Sea sediments appears to shift the microbial community towards utilising iron (oxyhydr)oxides as alternative oxidants for AOM (Egger et al., 2017). These iron (oxyhydr)oxides are common in the Gulf of Gdańsk (Kurowski et al., 2024). As indicated by higher concentrations of dissolved Fe²⁺ and Mn²⁺ and increased precipitation of authigenic carbonates, AOM in the MET1 area may be coupled to iron reduction (Rzepa et al., 2026). Furthermore, in northern Baltic Sea pockmarks, SGD-driven advection compresses redox and reaction zones, reduces organic matter accumulation, suppresses SMI development, and leads to archaeal communities dominated by AOA, whereas diffusion-dominated inactive pockmarks accumulate organic-rich sediments characterised by a prevalence of methanogens (Purkamo et al., 2022).

P/MET1-BH shows strong CH₄ enrichment and SO₄²⁻ depletion, indicating an active or recently active methane-influenced redox zone (Fig. 2). However, its GDGT concentrations are much lower than those in pockmarks P/MET3 and P/MET4. Conversely, P/MET3 shows substantial GDGT accumulation despite weaker porewater methane enrichment and a less pronounced archaeal presence involved

in CH₄ cycling. This decoupling suggests that the bulk GDGT pool integrates in situ archaeal production, contributions from sedimentary lineages such as Methanomicrobia, Methanosarcinia, Thermoplasmata, and possibly others and uncultivated archaea, together with pelagic input of Nitrososphaeria-derived crenarchaeol.

In pockmark P/MET4, the strongest porewater methane enrichment coincides with exceptionally high relative abundance of Methanosarcinaceae (Fig. 2, 8e) and below the SMI, with exceptionally high relative abundance of ANME-2a-2b (and ANME-2b at the genus level) (Figs. 8e, S6, S7a, b) and high sulphate concentration (Fig. 2), which indicates rather high productivity of this pockmark. At the same time, for the S/MET4 reference site, the low methane concentration of 0.011 mM is the highest throughout the profile and sulphate concentration remains high; however, the bottom-most sample of the archaeal community shows 0 reads (Fig. 8a), while in the upper part of the profile dominates uncultured lineages and Nanoarchaeia. Pockmark MET1-MP also shows pronounced enrichment of ANME-2a-2b at the deeper part of the profile below SMI (and ANME-2b at the genus level) (Figs. 8e, S6, S7a, b), and in the reference core, at the mid-depth of the profile below the shallow SMI, which may suggest deeper ANME zonation. Thus, methane-related communities are not limited to the pockmark core but extend into adjacent sediments. However, reference cores S/MET3 and S/MET4 do not show methanotrophic archaea (Fig. S9), which aligns with the low/absent CH₄ (Fig. 2). Ultimately, groundwater discharge influences microbial community composition by transporting microorganisms within sediments; however, prevailing environmental conditions and interactions determine which microorganisms become dominant (Justice et al., 2017).

4.4 Controls on archaeal lipid accumulation: methane cycling, LOI, and pockmark activity

The iGDGT distribution profiles offer an additional lipid-based perspective on the spatial heterogeneity of the investigated pockmark systems. Pockmark cores, particularly P/MET3 and P/MET4, show elevated concentrations of archaeal lipids \sum iGDGT and \sum OH-GDGT (Figs. 4, 6) relative to adjacent reference cores, indicating enhanced archaeal lipid accumulation in selected pockmark cores. In the pockmark core P/MET4, high iGDGT concentrations coincide with strong porewater CH₄ enrichment, SO₄²⁻ depletion (Fig. 2), lower Cl⁻ concentrations relative to the reference core (Fig. 2), and local enrichment of methane-cycling archaea (Fig. 8e), including ANME-2b, ANME-3, and methanogen-affiliated genera (Figs. S6a, b, S7, S8). Taken together, these suggest that CH₄ cycling and possibly weak porewater freshening contributed to the archaeal lipid signal. The elevated GDGT-3 concentration in pockmark P/MET4 is also consistent with a locally increased contribution from ANME-3

(at P/MET4/5; Fig. S7a), although GDGT-3 is not source-specific.

To assess whether elevated \sum iGDGT concentrations might simply reflect higher bulk organic matter content, GDGT profiles were compared with LOI-derived trends in organic matter (full-core elemental TOC data were not available for all sites) (Fig. S2). LOI was used as a screening-level proxy, supported by comparisons of measured TOC and LOI profiles in representative cores, which show comparable vertical trends (Supplementary material Fig. S2). The use of LOI as an organic matter proxy is supported by previous regional geochemical research by Łukawska-Matuszewska et al. (2014), based on a substantially larger sample set, which demonstrated a strong correlation ($R^2 = 0.68$) between LOI and organic carbon. The findings indicate that LOI is an effective screening tool for assessing geochemical variability related to organic matter.

This comparison indicates that \sum iGDGT and \sum OH-GDGT concentrations are not tightly coupled to bulk organic matter (Figs. 3, 4, 6, S2). In several cores, GDGT profiles do not align with LOI trends: for example, pockmark P/MET1-BH shows relatively high LOI and clear CH₄ enrichment with SO₄²⁻ depletion, yet does not exhibit the strongest GDGT accumulation, whereas pockmark P/MET3 contains elevated \sum iGDGT and \sum OH-GDGT concentrations despite weaker porewater CH₄ enrichment and a smaller contribution from methane-cycling archaea than P/MET4. The strong GDGT enrichment cannot be fully explained by elevated LOI across pockmark profiles, because the tetraether lipid maxima do not align with those of bulk organic matter. However, due to limitations of the LOI application, such as sensitivity to experimental conditions, interference from sediment composition, and loss of inorganic carbon, TOC measurements should be performed on the samples to verify the relationship between organic matter content and tetraether lipids.

Lipid preservation could potentially be a side effect of the less ebullitive nature of methane seepage in pockmarks P/MET3 and P/MET4, thereby enhancing CH₄ accumulation over time: the kinetics and episodicity of CH₄ supply to the seabed and of freshened porewater discharge are reduced in pockmarks P/MET3 and P/MET4 compared with those reported in previous studies (Idczak et al., 2020; Brodecka-Goluch et al., 2022; Łukawska-Matuszewska and Dwornik, 2025; Rzepa et al., 2026) for more hydrologically complex pockmarks of the MET1 area. Additionally, present-day dissolved CH₄ and SO₄²⁻ profiles may not fully capture the temporal geochemical variability of this environment. As reported by Treude et al. (2005), the spatial and temporal heterogeneity caused by gas ebullition allows methanogens and sulphate reducers to coexist in Eckernförde Bay, feeding the shallow SMI, but also enables CH₄ to escape into the overlying water column, bypassing the microbial barrier.

4.5 Limitations of GDGT-based AOM proxies in ANME-2/ANME-3-dominated pockmarks of the Gdańsk Basin

Peaks in archaeal abundance (Fig. S10) and in GDGT concentrations at sediment depths of 5–45 cm could mark the SMI (Fig. 2). However, iGDGTs indices (Table 1; Fig. S3) do not support a strong AOM imprint, as values remain uniformly low. MI values (< 0.09) fall well below the 0.3–0.5 threshold indicative of CH_4 -impacted sediments observed by Zhang et al. (2011). However, for the MI value to reach 0.5, methanotrophic-derived GDGT must constitute approximately 30%–50% of the total GDGT pool (Kim and Zhang, 2023).

A low MI index, calculated as the ratio of GDGT-1-3 to crenarchaeol, typically indicates minimal methanotrophic contribution relative to Nitrososphaeria-derived sources (Zhang et al., 2011). The uniformly low MI values observed here likely reflect a strong crenarchaeol signal from ammonia-oxidising archaea thriving above, in the water column and/or limited GDGT-1-3 production by the dominant AOM lineages, rather than definitively excluding AOM. GDGT-1 to -3, which increase substantially in ANME-1-dominated systems (Rossel et al., 2008), are two orders of magnitude less abundant in the analysed samples than GDGT-0 and crenarchaeol, consistent with the near-absence of ANME-1 (maximum relative abundance of 0.6% in S/MET3/5; Fig. 8a).

Although the applicability of MI to ANME-2 and ANME-3 (which dominate the AOM community here; Fig. S8) has been questioned, comprehensive biomarker investigations generally support its utility for AOM detection (Kim and Zhang, 2023). Nevertheless, ANME-2 and ANME-3 alone are unlikely to contribute substantially to GDGT production (Niemann and Elvert, 2008; Weijers et al., 2011), making MI non-diagnostic in this study. The consistently low GDGT-2 / cren ratios (maximum 0.04; Table 1) support this interpretation. This ratio typically indicates CH_4 -rich AOM conditions, under which ANME-1-synthesised GDGT-2 (Rossel et al., 2008) is elevated relative to crenarchaeol. To further evaluate the GDGT distribution characteristics of an AOM-related SMI, the relative abundances of GDGT-1, GDGT-2, and GDGT-3 were compared across cores. In contrast to the GDGT-2-dominated pattern reported by Weijers et al. (2011), GDGT-2 was not the dominant compound in any of our samples. Instead, 74 of 75 samples showed the order GDGT-1 > GDGT-2 > GDGT-3. This indicates that the investigated cores do not show enrichment of GDGT-2, consistent with uniformly low GDGT-2 / crenarchaeol ratios.

Nevertheless, ANME lineages are more prevalent in pockmark cores (Fig. S9), suggesting, relatively to reference cores, enhanced AOM activity, particularly at P/MET3 and P/MET4. Peaks in GDGT-1 to -3 concentrations also occur in reference cores, following the general trend for all iGDGTs, but at lower concentrations (Fig. S4). In addition, certain

core GDGTs (e.g., GDGT-1) may arise from diagenetic and degradative processes acting on phosphohexose headgroups predominantly produced by *Ca. Nitrosopumilus* in the Baltic Sea (Wittenborn et al., 2023).

Overall, AOM activity appears shallow within the studied pockmarks, consistent with previous investigations demonstrating weak S-AOM confined to thin, shallow sediment layers and potentially dependent on alternative electron acceptors in deeper layers (Broclawik et al., 2020; Idczak et al., 2020; Brodecka-Goluch et al., 2022; Łukawska-Matuszewska et al., 2022; Ehlert von Ahn et al., 2024). The minor contribution of *Ca. Methanoperedens* in the dataset (MET1-MP; Fig. S9) indicates traces of AOM coupled to nitrate and/or metal oxide reduction. Members of the family Methanoperedenaceae (formerly ANME-2D) typically inhabit sulphate-depleted freshwater systems and perform AOM independently of syntrophic partnerships (Haroon et al., 2013; Ettwig et al., 2016; Vaksmaa et al., 2017; Leu et al., 2020).

4.6 Methanogens and GDGT-based proxies

Within the CH_4 -cycling archaeal community, methanogens appear to be the primary contributors to GDGT biosynthesis (Fig. 5). Although GDGT-0 and crenarchaeol predominate in marine sediments (Schouten et al., 2002), their elevated concentrations across all investigated gas systems indicate that they serve as primary iGDGT biomarkers in the sediments of the Gdańsk Basin, even in CH_4 -rich settings harbouring both methanogenic and methanotrophic communities. However, GDGT-0 lacks source specificity and can be synthesised by multiple archaeal lineages, including methanogens and methanotrophs (Pancost et al., 2001; Blaga et al., 2009; Inglis et al., 2015; Słowakiewicz et al., 2016; Petrick et al., 2019). These lineages may also produce cyclised GDGTs (Koga et al., 1993; Weijers et al., 2006; Schouten et al., 2013; Bauersachs et al., 2015), although this is not always replicable in culture studies (Bauersachs et al., 2015).

The network analysis indicates that AOA-associated crenarchaeol and the statistically co-varying GDGT-0 are the primary drivers of variation in the bulk GDGT pool (Fig. 9), likely masking the methanogen signal by influencing the GDGT-0 / cren ratio through crenarchaeol contribution from pelagic Nitrososphaeria. The observed GDGT-0 / cren ratios in Gdańsk Basin samples are < 0.99 , well below the 2 threshold characteristic of methanogen-dominated systems (Schouten et al., 2002; Blaga et al., 2009), indicating minimal methanogen contribution and AOA predominance. In the northern Baltic Sea pockmarks (Hanko Basin), Nitrososphaeria – including some groundwater-origin populations – constitute a major component of the archaeal community (Purkamo et al., 2022), consistent with evidence that *Ca. Nitrosopumilus* is a widespread, important GDGT-producing lineage in the Baltic Sea (Wittenborn et al., 2023). However, sedimentary iGDGTs integrate archaeal lipid production and

export over longer timescales, and their distribution is further shaped by preservation conditions (Lengger et al., 2013), while in contrast, amplicon-based relative abundance reflects the compositional distribution of recovered 16S rRNA gene reads after DNA extraction (Gloor et al., 2017) and does not directly indicate lipid production rates.

4.7 AOA and non-methane archaeal lipid sources

Given that AOA are abundant in the Baltic Sea under low-oxygen conditions and along redox gradients (Berg et al., 2015b), GDGT-0/cren ratios (< 1) and very high abundance of *Ca. Nitrosopumilus* in both pockmark and reference sediment cores (Fig. S7), suggest a substantial contribution of crenarchaeol most likely originating from the water column. Although our samples do not represent the archaeal community in the source groundwater and were collected during a single season, the groundwater-associated Nitrososphaeria reported by Purkamo et al. (2022), such as *Nitrosoarchaeum* or *Ca. Nitrosotalea*, were not identified. Instead, Nitrososphaeria is represented only by *Ca. Nitrosopumilus*, a major AOA taxon in the Baltic Sea water column (Wittenborn et al., 2023, with references therein), therefore supporting pelagic AOA origin of crenarchaeol in the studied samples.

Methane seepage creates chemically reducing conditions that limit the growth of oxygen-dependent organisms. However, AOA can persist and function (Jakobs et al., 2016) in sharp chemical gradients and microenvironments (e.g., thin oxic/suboxic boundary layers). Martens-Habbena and Qin (2022) showed that *Nitrosopumilus maritimus* can sustain ammonia oxidation under oxygen-depleted conditions, further indicating that AOA may be flexible and physiologically adapted to redox-variable conditions.

Nevertheless, elevated summed iGDGT and OH-GDGT concentrations in pockmarks P/MET3 and P/MET4 (especially GDGT-0 and crenarchaeol; Figs. 4–7) may indicate an indirect ecological linkage between the nitrogen and carbon biogeochemical cycles in the studied system, in which sulphate reduction, degradation of organic matter, methanogenesis, and other anaerobic processes release NH_4^+ and other reduced compounds into porewaters. These compounds may subsequently be transported (diffused) into the bottom waters and the overlying water column, where Nitrososphaeria thrive. Consequently, crenarchaeol remains the dominant iGDGT in both pockmark and reference cores (Fig. S4), as Nitrososphaeria is abundant in the overlying water column and may feed on the products of enhanced processes occurring in the sediments.

Thus, intensified organic matter degradation may influence GDGT accumulation, as evidenced by the GDGT profiles of pockmarks P/MET3 and P/MET4 in the Gdańsk Deep, which are characterised by historically documented weak or absent seabed activity (Fig. S1, Table S1), in contrast to the seabed activity observed at pockmark MET1. To better investigate

organic matter degradation in the studied pockmarks, porewater alkalinity and ammonia concentrations should be measured concurrently with GDGTs. However, the particularly high Σ iGDGT and Σ OH-GDGT concentrations in pockmark P/MET4 coincide with the highest porewater concentrations of CH_4 and SO_4^{2-} and with the most abundant and diverse CH_4 -cycling archaeal community among the sites examined. This may imply elevated primary productivity and the deposition of organic matter that settles on the seafloor, which fuels decomposition and methanogenesis in the sediments, but also indicates thriving conditions for Thaumarchaeota in the water column. Despite the AOA dominance recorded in crenarchaeol concentration and very high relative abundance of *Ca. Nitrosopumilus* (Fig. S7), GDGT-0 concentrations remain relatively elevated across the pockmark sites, particularly at the inactive pockmark P/MET3 and the weakly active pockmark P/MET4, which experiences weak, occasional porewater seepage, compared with active venting systems characterised by focused CH_4 flow, such as mud volcanoes on the Canadian Beaufort Sea slope (Lee et al., 2018) and studied here pockmarks MET1-MP and MET1-BH (Fig. S4).

Average OH-GDGT% values align with those reported for Baltic Sea surface sediments (Sinninghe Damsté et al., 2022), and RI-OH and RI-OH' values are within the Baltic/Skagerrak Surface sediment ranges (Sinninghe Damsté et al., 2022). While salinity primarily controls OH-GDGT behaviour (Sinninghe Damsté et al., 2022), recent studies show strong responses to nitrate availability and water-column stratification (Harning and Sepúlveda, 2024), indicating an ecological influence on RI-OH/RI-OH'. The most robust interpretation is that OH-GDGTs primarily track AOA, particularly Nitrososphaeria, as supported by culture studies (Sinninghe Damsté et al., 2022). In our data, OH-GDGTs closely covary with crenarchaeol, consistent with previous findings indicating thaumarchaeotal source (Kaiser and Arz, 2016).

Furthermore, Nanoarchaeota, prevalent across the samples, may be involved in ectosymbiosis with Nitrososphaeria, consistent with their reliance on symbiotic relationships (Waters et al., 2003). Nanoarchaeota may also possess GDGTs, previously attributed to their biological hosts (Zeng et al., 2022), which could explain their correlation with GDGTs (Fig. 9). They can also associate with methanogens (Brick et al., 2025), which may explain their high relative abundance ($\sim 40\%$ in non-pockmark and $\sim 55\%$ in pockmark sediments). Other frequent groups, e.g., AR15 and AR20, are likewise symbiotic or parasitic; the latter, linked to groundwater (Castelle et al., 2015), could underscore the influence of porewater freshening in the Gulf of Gdańsk in pockmarks MET1-MP and MET1-BH.

Several archaeal groups, including Thermoplasmata, Bathyarchaeia, Lokiarchaeia, Heimdallarchaeia, Archaeoglobi, and the Deep Sea Euryarchaeotic Group (DSEG; within Thermoplasmata; Rinke et al., 2021), are associated with

the degradation of complex organic matter, aromatic carbon degradation, protein catabolism, and fermentation (Zinke et al., 2019). These groups – particularly Bathyarchaeia and Thermoplasmata – are more abundant in reference cores than in pockmarks and may contribute to GDGT production in anoxic environments (Besseling et al., 2018, 2020; Baxter et al., 2021). Bathyarchaeia thrive in anoxic environments, degrading recalcitrant organic matter (Baxter and Zalar, 2019; Blewett et al., 2022; Zeng et al., 2022), whereas Archaeoglobi mediate both sulphate reduction and methanogenesis (Lynes et al., 2024). Bathyarchaeia may also occupy a central position in archaeal carbon-nitrogen networks, co-occurring with methanogens and Nitrososphaeria, and potentially linking organic carbon degradation with reduced nitrogen availability (Yi et al., 2024). However, despite the abundance of Bathyarchaeia and Nitrososphaeria in the archaeal community structure, this mechanism remains inferential, as NH_4^+ and AOA activity were not directly measured herein. Asgard archaea, including hydrocarbon-degrading Lokiarchaeia and hydrogen-dependent acetogenic Heimdalarchaeia (Zhang et al., 2025), also show higher abundance in reference cores and may contribute to iGDGT production, likely GDGT0 (Zeng et al., 2022). Although the tetraether synthase (Tes) gene, essential for GDGT biosynthesis, has been identified in Hadarchaeia and Altiarchaeia, GDGTs have not yet been detected in these groups (Zeng et al., 2022). Notably, some Hadarchaeia grow syntrophically with methanogens (Yu et al., 2024). Interestingly, Thermococci which is known to produce GDGT-0 (Zeng et al., 2022), has not been resolved at lower taxonomic levels in our samples, but shows high abundance in pockmarks (Fig. 8a).

5 Conclusions

This study presents the first integrated analysis of archaeal 16S rRNA communities, sedimentary iGDGT/OH-GDGT distributions, and microbial correlation networks in methane pockmarks of the Gdańsk Basin. Pockmarks host more diverse and abundant archaeal communities than adjacent reference sites, and due to correlation network, function as tightly coupled metabolic systems, whereas reference sites exhibit more niche-partitioned ecological structures. Despite CH_4 -rich conditions, evidence for AOM remains limited. Low MI values and the near absence of ANME-1 reduce the reliability of GDGT-based AOM proxies in studied settings. Low GDGT-0 / cren and GDGT-2 / cren ratios indicate dominance of pelagic AOA, particularly *Ca. Nitrosopumilus*, which may mask methanogenic GDGT signals, but do not support a groundwater origin for Nitrososphaeria in the studied gas systems, as hypothesised for pockmarks in Hanko Bay, Baltic Sea. However, the dominance of GDGT-0 and crenarchaeol in specific pockmarks may reveal intricate linkages between microbial community structure (i.e., Bathyarchaeia and Nitrososphaeria) and the underlying bio-

geochemical processes. The transport of reduced compounds from anaerobic reactions across the sediment-water interface may enhance the proliferation of Nitrososphaeria.

The mixing of freshened groundwater with marine pore-water, together with gas seepage, may indicate localised microbial “hotspots” with higher archaeal diversity. Our findings show that pockmarks in the Gdańsk Basin can act as spatially heterogeneous and temporally variable hotspots of archaeal activity, with community composition reflecting the intensity of the methane-cycling reaction zone, which develops where local geochemical gradients favour methanogenesis and AOM, irrespective of whether seabed gas escape is strongly expressed at the time of observation. Differences between active (P/MET1) and inactive (P/MET3) or weakly active (P/MET4) pockmarks are reflected in archaea abundance, methane-cycling archaeal community structure, and Σ iGDGT concentrations, but the relationship is non-linear. Pockmark P/MET4 shows a strong CH_4 -cycling archaeal signal despite being only weakly active at the seabed, which can indicate the importance of subsurface conditions for methane production, as well as for the accumulation, decomposition, and mineralisation of organic matter; while active pockmark MET1-BH may lose CH_4 through periodic, strong, and focused gas and water seepage and potential gas escape.

Our study defines the conditions and limitations under which iGDGTs can be interpreted in Baltic Sea pockmarks. Local CH_4 -driven processes do not fundamentally alter the sedimentary tetraether lipid record, which instead reflects the broader marine environmental signal. The clearest combined biomarker, geochemical, and microbiological evidence for methane cycling, observed mostly at pockmark P/MET4, indicates increased iGDGT concentrations, elevated CH_4 , depleted SO_4^{2-} , and shallow SMI, along with enrichment of ANME-2b, ANME-3, hydrogenotrophic methanogens, and where *Methanosarcina*, *Methanosaeta*, and *Methanoregula* co-occur. However, the iGDGT distribution in the weakly active pockmark P/MET4 is similar to that of the adjacent reference sediments, probably indicating a pelagic AOA source. The inactive pockmark P/MET3 also shows increased accumulation of archaeal tetraether lipids compared with the reference core. As in pockmark P/MET4, the iGDGT distribution is primarily associated with water-column processes of pelagic AOA rather than with processes driven by CH_4 -cycling communities in the sediment, as evidenced by the dominance of crenarchaeol. Active MET1 pockmarks also show iGDGT distributions similar to those of adjacent reference cores, so the differences between pockmarks lie in the concentration of iGDGTs rather than in their distribution. Therefore, the concentration profiles of iGDGT and OH-GDGT could perhaps serve as a proxy for primary productivity in the Baltic Sea.

Future studies should integrate GDGT analyses with methane-specific biomarkers (e.g., crocetane, PMI, archaeol, hydroxyarchaeol), NH_4^+ concentrations, porewater alkalinity, compound-specific carbon isotopes, and functional gene or

transcriptomic approaches (e.g., *mcrA*) to better constrain active CH₄ cycling and identify the responsible ANME clades, as well as spatial activity of Nitrososphaeria. Measuring both core and intact polar lipids in sediments and the water column would further clarify GDGT production, transport, and preservation. Overall, this study highlights the need for integrated multi-proxy and multi-omic approaches to distinguish active microbial processes from preserved diagenetic signals in methane seep systems influenced by submarine groundwater discharge, porewater freshening, and dynamic redox conditions.

Data availability. All iGDGT data is available in the repository <https://doi.org/10.5281/zenodo.18414700> (De Mey-Śnieżyńska, 2026).

Supplement. The supplement related to this article is available online at <https://doi.org/10.5194/bg-23-4485-2026-supplement>.

Author contributions. IDMS and MS designed the research; IDMS evaluated the geochemical and microbiological data; AB, ABG, and KLM collected the samples; AB prepared the microbiological dataset; IDMS and AB conducted the statistical analyses; IDMS wrote the manuscript; FP and MS reviewed and edited the manuscript.

Competing interests. The contact author has declared that none of the authors has any competing interests.

Disclaimer. Publisher's note: Copernicus Publications remains neutral with regard to jurisdictional claims made in the text, published maps, institutional affiliations, or any other geographical representation in this paper. The authors bear the ultimate responsibility for providing appropriate place names. Views expressed in the text are those of the authors and do not necessarily reflect the views of the publisher.

Acknowledgements. This study was partially funded by the Elsevier Research Scholarship (awarded to IDMS). IDMS is grateful to the Organic Geochemistry Group at Utrecht University for assistance with analyses. AB, ABG, and KLM thank the captain and crew of RV *Oceanograf* for their support during the cruises. Paweł Działałak is thanked for isolating material for DNA analysis. We are also grateful to the handling editor, Sophie ten Hietbrink and one anonymous reviewer for their detailed and helpful comments.

Financial support. This research has been partially supported by the subsidy granted to the AGH University of Krakow by the Ministry of Science and Higher Education (grant no. 16.16.140.315).

Review statement. This paper was edited by Sebastian Naeher and reviewed by Sophie ten Hietbrink and one anonymous referee.

References

- Adam-Beyer, N., Deusner, C., Schmidt, M., and Perner, M.: Microbial hydrogen oxidation potential in seasonally hypoxic Baltic Sea sediments, *Front. Microbiol.*, 16, <https://doi.org/10.3389/fmicb.2025.1565157>, 2025.
- Aitchison, J.: The statistical analysis of compositional data, *J. R. Stat. Soc. Ser. B Methodol.*, 44, 139–160, <https://doi.org/10.1111/j.2517-6161.1982.tb01195.x>, 1982.
- Bale, N. J., Palatinszky, M., Rijpstra, W. I. C., Herbold, C. W., Wagner, M., and Sinninghe Damsté, J. S.: Membrane lipid composition of the moderately thermophilic ammonia-oxidizing archaeon “*Candidatus Nitrosotenuis uzonensis*” at different growth temperatures, *Appl. Environ. Microbiol.*, 85, e01332-19, <https://doi.org/10.1128/AEM.01332-19>, 2019.
- Bauersachs, T., Weidenbach, K., Schmitz, R. A., and Schwark, L.: Distribution of glycerol ether lipids in halophilic, methanogenic and hyperthermophilic archaea, *Org. Geochem.*, 83–84, 101–108, <https://doi.org/10.1016/j.orggeochem.2015.03.009>, 2015.
- Baxter, A. J., van Bree, L. G. J., Peterse, F., Hopmans, E. C., Villanueva, L., Verschuren, D., and Sinninghe Damsté, J. S.: Seasonal and multi-annual variation in the abundance of isoprenoid GDGT membrane lipids and their producers in the water column of a meromictic equatorial crater lake (Lake Chala, East Africa), *Quat. Sci. Rev.*, 273, 107263, <https://doi.org/10.1016/j.quascirev.2021.107263>, 2021.
- Baxter, B. K. and Zalar, P.: The extremophiles of Great Salt Lake: Complex microbiology in a dynamic hypersaline ecosystem, in: *Model Ecosystems in Extreme Environments*, edited by: Seckbach, J. and Rampelotto, P., Academic Press, 57–99, <https://doi.org/10.1016/B978-0-12-812742-1.00004-0>, 2019.
- Berg, C., Listmann, L., Vandieken, V., Vogts, A., and Jürgens, K.: Chemoautotrophic growth of ammonia-oxidizing Thaumarchaeota enriched from a pelagic redox gradient in the Baltic Sea, *Front. Microbiol.*, 5, <https://doi.org/10.3389/fmicb.2014.00786>, 2015a.
- Berg, C., Vandieken, V., Thamdrup, B., and Jürgens, K.: Significance of archaeal nitrification in hypoxic waters of the Baltic Sea, *ISME J.*, 9, 1319–1332, <https://doi.org/10.1038/ismej.2014.218>, 2015b.
- Besseling, M. A., Hopmans, E. C., Boschman, R. C., Sinninghe Damsté, J. S., and Villanueva, L.: Benthic archaea as potential sources of tetraether membrane lipids in sediments across an oxygen minimum zone, *Biogeosciences*, 15, 4047–4064, <https://doi.org/10.5194/bg-15-4047-2018>, 2018.
- Besseling, M. A., Hopmans, E. C., Bale, N. J., Schouten, S., Damsté, J. S., and Villanueva, L.: The absence of intact polar lipid-derived GDGTs in marine waters dominated by Marine Group II: Implications for lipid biosynthesis in Archaea, *Sci. Rep.*, 10, 294, <https://doi.org/10.1038/s41598-019-57035-0>, 2020.
- Bijl, P. K., Śliwińska, K. K., Duncan, B., Hugué, A., Naeher, S., Rattanasriampai, R., Sosa-Montes de Oca, C., Auderset, A., Berke, M. A., Kim, B. S., Davtian, N., Dunkley Jones, T., Eefting, D. D., Elling, F. J., Fenies, P., Inglis, G. N., O'Connor,

- L., Pancost, R. D., Peterse, F., Rice, A., Sluijs, A., Varma, D., Xiao, W., and Zhang, Y. G.: Reviews and syntheses: Best practices for the application of marine GDGTs as proxy for paleotemperatures: sampling, processing, analyses, interpretation, and archiving protocols, *Biogeosciences*, 22, 6465–6508, <https://doi.org/10.5194/bg-22-6465-2025>, 2025.
- Blaga, C. I., Reichart, G.-J., Heiri, O., and Sinninghe Damsté, J. S.: Tetraether membrane lipid distributions in water-column particulate matter and sediments: a study of 47 European lakes along a north–south transect, *J. Paleolimnol.*, 41, 523–540, <https://doi.org/10.1007/s10933-008-9242-2>, 2009.
- Blainey, P. C., Mosier, A. C., Potanina, A., Francis, C. A., and Quake, S. R.: Genome of a low-salinity ammonia-oxidizing archaeon determined by single-cell and metagenomic analysis, *PLoS One*, 6, e16626, <https://doi.org/10.1371/journal.pone.0016626>, 2011.
- Blewett, J., Elling, F. J., Naafs, B. D. A., Kattein, L., Evans, T. W., Lauretano, V., Gallego-Sala, A. V., Pancost, R. D., and Pearson, A.: Metabolic and ecological controls on the stable carbon isotopic composition of archaeal (isoGDGT and BDGT) and bacterial (brGDGT) lipids in wetlands and lignites, *Geochim. Cosmochim. Acta*, 320, 1–25, <https://doi.org/10.1016/j.gca.2021.12.023>, 2022.
- Blondel, V. D., Guillaume, J.-L., Lambiotte, R., and Lefebvre, E.: Fast unfolding of communities in large networks, *J. Stat. Mech.: Theory Exp.*, 2008, P10008, <https://doi.org/10.1088/1742-5468/2008/10/P10008>, 2008.
- Boetius, A., Ravensschlag, K., Schubert, C. J., Rickert, D., Widel, F., Gieseke, A., Amann, R., Jørgensen, B. B., Witte, U., and Pfannkuche, O.: A marine microbial consortium apparently mediating anaerobic oxidation of methane, *Nature*, 407, 623–626, <https://doi.org/10.1038/35036572>, 2000.
- Brick, S., Niggemann, J., Reckhardt, A., Könneke, M., and Engelen, B.: Interstitial microbial communities of coastal sediments are dominated by Nanoarchaeota, *Front. Microbiol.*, 16, 1532193, <https://doi.org/10.3389/fmicb.2025.1532193>, 2025.
- Broclawik, O., Łukawska-Matuszewska, K., Brodecka-Goluch, A., and Bolalek, J.: Impact of methane occurrence on iron speciation in the sediments of the Gdansk Basin (Southern Baltic Sea), *Sci. Tot. Environ.*, 721, 137718, <https://doi.org/10.1016/j.scitotenv.2020.137718>, 2020.
- Brodecka, A., Majewski, P., Bolalek, J., and Klusek, Z.: Geochemical and acoustic evidence for the occurrence of methane in sediments of the Polish sector of the southern Baltic Sea*, *Oceanologia*, 55, 951–978, <https://doi.org/10.5697/oc.55-4.951>, 2013.
- Brodecka-Goluch, A., Idczak, J., Gorska, N., and Bolalek, J.: Geophysical and geochemical characteristics of four different pockmark sites located in the Gdańsk Basin, in: 3rd Baltic Earth Conference “Earth system changes and Baltic Sea coasts”, 1–5 June 2020, Jastarnia, pp. 89–90, 2020.
- Brodecka-Goluch, A., Łukawska-Matuszewska, K., Kotarba, M. J., Borkowski, A., Idczak, J., and Bolalek, J.: Biogeochemistry of three different shallow gas systems in continental shelf sediments of the South-Eastern Baltic Sea (Gulf of Gdańsk): Carbon cycling, origin of methane and microbial community composition, *Chem. Geol.*, 597, 120799, <https://doi.org/10.1016/j.chemgeo.2022.120799>, 2022.
- Burnett, W. C., Bokuniewicz, H., Huettel, M., Moore, W. S., and Taniguchi, M.: Groundwater and pore water inputs to the coastal zone, *Biogeochemistry*, 66, 3–33, <https://doi.org/10.1023/B:BIOG.0000006066.21240.53>, 2003.
- Burnett, W. C., Aggarwal, P. K., Aureli, A., Bokuniewicz, H., Cable, J. E., Charette, M. A., Kontar, E., Krupa, S., Kulkarni, K. M., Loveless, A., Moore, W. S., Oberdorfer, J. A., Oliveira, J., Ozyurt, N., Povinec, P., Privitera, A. M. G., Rajar, R., Ramesur, R. T., Scholten, J., Stieglitz, T., Taniguchi, M., and Turner, J. V.: Quantifying submarine groundwater discharge in the coastal zone via multiple methods, *Sci. Tot. Environ.*, 367, 498–543, <https://doi.org/10.1016/j.scitotenv.2006.05.009>, 2006.
- Bussmann, I. and Suess, E.: Groundwater seepage in Eckernförde Bay (Western Baltic Sea): Effect on methane and salinity distribution of the water column, *Cont. Shelf Res.*, 18, 1795–1806, [https://doi.org/10.1016/S0278-4343\(98\)00058-2](https://doi.org/10.1016/S0278-4343(98)00058-2), 1998.
- Callow, B., Bull, J. M., Provenzano, G., Böttner, C., Birinci, H., Robinson, A. H., Henstock, T. J., Minshull, T. A., Bayrakci, G., Lichtschlag, A., Roche, B., Yilo, N., Gehrmann, R., Karstens, J., Falcon-Suarez, I. H., and Berndt, C.: Seismic chimney characterisation in the North Sea – Implications for pockmark formation and shallow gas migration, *Mar. Pet. Geol.*, 133, 105301, <https://doi.org/10.1016/j.marpetgeo.2021.105301>, 2021.
- Carman, R. and Jonsson, P.: Distribution patterns of different forms of phosphorus in some surficial sediments of the Baltic Sea, *Chem. Geol.*, 90, 91–106, [https://doi.org/10.1016/0009-2541\(91\)90036-Q](https://doi.org/10.1016/0009-2541(91)90036-Q), 1991.
- Carstensen, J., Conley, D. J., Bonsdorff, E., Gustafsson, B. G., Hietanen, S., Janas, U., Jilbert, T., Maximov, A., Norkko, A., Norkko, J., Reed, D. C., Slomp, C. P., Timmermann, K., and Voss, M.: Hypoxia in the Baltic Sea: biogeochemical cycles, benthic fauna, and management, *AMBIO*, 43, 26–36, <https://doi.org/10.1007/s13280-013-0474-7>, 2014.
- Castelle, C. J., Wrighton, K. C., Thomas, B. C., Hug, L. A., Brown, C. T., Wilkins, M. J., Frischkorn, K. R., Tringe, S. G., Singh, A., Markillie, L. M., Taylor, R. C., Williams, K. H., and Banfield, J. F.: Genomic expansion of domain Archaea highlights roles for organisms from new phyla in anaerobic carbon cycling, *Curr. Biol.*, 25, 690–701, <https://doi.org/10.1016/j.cub.2015.01.014>, 2015.
- Chen, S., Zhou, Y., Chen, Y., and Gu, J.: fastp: an ultra-fast all-in-one FASTQ preprocessor, *Bioinformatics*, 34, i884–i890, <https://doi.org/10.1093/bioinformatics/bty560>, 2018.
- Conklin, A., Stensel, H. D., and Ferguson, J.: Growth kinetics and competition between *Methanosarcina* and *Methanosaeta* in mesophilic anaerobic digestion, *Water Environ. Res.*, 78, 486–496, <https://doi.org/10.2175/106143006X95393>, 2006.
- De Mey-Śnieżyńska, I.: Gdansk Basin iGDGT OH-GDGT Holocene marine sediment cores, Zenodo [data set], <https://doi.org/10.5281/zenodo.18414700>, 2026.
- De Rosa, M., De Rosa, S., Gambacorta, A., Minale, L., and Bu'lock, J. D.: Chemical structure of the ether lipids of thermophilic acidophilic bacteria of the *Caldariella* group, *Phytochemistry*, 16, 1961–1965, [https://doi.org/10.1016/0031-9422\(77\)80105-2](https://doi.org/10.1016/0031-9422(77)80105-2), 1977.
- De Vrieze, J.: *Methanosaeta* vs. *Methanosarcina* in anaerobic digestion: the quest for enhanced biogas production, PhD dissertation, Ghent University, <https://biblio.ugent.be/publication/5704591> (last access: 1 July 2026), 2014.
- Dearing Crampton-Flood, E., Peterse, F., and Sinninghe Damsté, J. S.: Production of branched tetraethers in the marine realm:

- Svalbard fjord sediments revisited, *Org. Geochem.*, 138, 103907, <https://doi.org/10.1016/j.orggeochem.2019.103907>, 2019.
- Díaz-Mendoza, G. A., Krämer, K., von Rönn, G. A., Schwarzer, K., Heinrich, C., Reimers, H.-C., and Winter, C.: Circular structures on the seabed: differentiating between natural and anthropogenic origins – Examples from the Southwestern Baltic Sea, *Front. Earth Sci.*, 11, 1170787, <https://doi.org/10.3389/feart.2023.1170787>, 2023.
- Ding, S., Kohlhepp, B., Trumbore, S., Küsel, K., Totsche, K.-U., Pohnert, G., Gleixner, G., and Schwab, V. F.: In situ production of core and intact bacterial and archaeal tetraether lipids in groundwater, *Org. Geochem.*, 126, 1–12, <https://doi.org/10.1016/j.orggeochem.2018.10.005>, 2018.
- Egger, M., Hagens, M., Sapart, C. J., Dijkstra, N., van Helmond, N. A. G. M., Mogollón, J. M., Risgaard-Petersen, N., van der Veen, C., Kasten, S., Riedinger, N., Böttcher, M. E., Röckmann, T., Jørgensen, B. B., and Slomp, C. P.: Iron oxide reduction in methane-rich deep Baltic Sea sediments, *Geochim. Cosmochim. Acta*, 207, 256–276, <https://doi.org/10.1016/j.gca.2017.03.019>, 2017.
- Ehlert von Ahn, C. M., Dellwig, O., Szymczycha, B., Kotwicki, L., Rooze, J., Endler, R., Escher, P., Schmiedinger, I., Sültenfuß, J., Diak, M., Gehre, M., Struck, U., Vogler, S., and Böttcher, M. E.: Submarine groundwater discharge into a semi-enclosed coastal bay of the southern Baltic Sea: A multi-method approach, *Oceanologia*, 66, 111–138, <https://doi.org/10.1016/j.oceano.2024.01.001>, 2024.
- Elling, F. J., Könneke, M., Nicol, G. W., Stieglmeier, M., Bayer, B., Spieck, E., de la Torre, J. R., Becker, K. W., Thomm, M., Prosser, J. I., Herndl, G. J., Schleper, C., and Hinrichs, K.-U.: Chemotaxonomic characterisation of the thaumarchaeal lipidome, *Environ. Microbiol.*, 19, 2681–2700, <https://doi.org/10.1111/1462-2920.13759>, 2017.
- Engvall, A.-G.: The fate of nitrogen in early diagenesis of Baltic sediments: a study of the sediment-water interface, PhD thesis, University of Stockholm, Stockholm, 16 pp., https://search.uu.se/discovery/fulldisplay?vid=46LIBRIS_UUB:UUB&docid=alma991000068279707596&lang=en&context=L (last access: 1 July 2026), 1978.
- Ettwig, K. F., Zhu, B., Speth, D., Keltjens, J. T., Jetten, M. S. M., and Kartal, B.: Archaea catalyze iron-dependent anaerobic oxidation of methane, *Proc. Natl. Acad. Sci. USA*, 113, 12792–12796, <https://doi.org/10.1073/pnas.1609534113>, 2016.
- Fenies, P., Ho, S. L., Hefter, J., and Lee, P.-T.: Impact of anaerobic methanotrophic archaeal input on hydroxylated isoprenoid GDGT-derived temperatures, *Org. Geochem.*, 218, 105213, <https://doi.org/10.1016/j.orggeochem.2026.105213>, 2026.
- Galagan, J. E., Nusbaum, C., Roy, A., Endrizzi, M. G., Macdonald, P., FitzHugh, W., Calvo, S., Engels, R., Smirnov, S., Atnoor, D., Brown, A., Allen, N., Naylor, J., Stange-Thomann, N., DeArellano, K., Johnson, R., Linton, L., McEwan, P., McKernan, K., Talamas, J., Tirrell, A., Ye, W., Zimmer, A., Barber, R. D., Cann, I., Graham, D. E., Grahame, D. A., Guss, A. M., Hedderich, R., Ingram-Smith, C., Kuettner, H. C., Krzycki, J. A., Leigh, J. A., Li, W., Liu, J., Mukhopadhyay, B., Reeve, J. N., Smith, K., Springer, T. A., Umayam, L. A., White, O., White, R. H., Conway de Macario, E., Ferry, J. G., Jarrell, K. F., Jing, H., Macario, A. J. L., Paulsen, I., Pritchett, M., Sowers, K. R., Swanson, R. V., Zinder, S. H., Lander, E., Metcalf, W. W., and Birren, B.: The genome of *M. acetivorans* reveals extensive metabolic and physiological diversity, *Genome Res.*, 12, 532–542, <https://doi.org/10.1101/gr.223902>, 2002.
- Gloor, G. B., Macklaim, J. M., Pawlowsky-Glahn, V., and Egozcue, J. J.: Microbiome datasets are compositional: and this is not optional, *Front. Microbiol.*, 8, 2224, <https://doi.org/10.3389/fmicb.2017.02224>, 2017.
- González-Toril, E., Gómez, F., Malki, M., and Amils, R.: The isolation and study of Acidophilic microorganisms, in: *Methods in Microbiology*, vol. 35, Academic Press, 471–510, [https://doi.org/10.1016/S0580-9517\(08\)70023-0](https://doi.org/10.1016/S0580-9517(08)70023-0), 2006.
- Guan, H., Liu, L., Birgel, D., Peckmann, J., Feng, D., and Li, S.: Hydroxylated GDGTs-0 in marine methane seep environments: A putative indicator for archaeal methanogenesis, *Org. Geochem.*, 198, 104862, <https://doi.org/10.1016/j.orggeochem.2024.104862>, 2024.
- Harning D. J. and Sepúlveda J.: Impact of non-thermal variables on hydroxylated GDGT distributions around Iceland, *Front. Earth Sci.*, 12, 1430441, <https://doi.org/10.3389/feart.2024.1430441>, 2024.
- Haroon, M. F., Hu, S., Shi, Y., Imelfort, M., Keller, J., Hugenholtz, P., Yuan, Z., and Tyson, G. W.: Anaerobic oxidation of methane coupled to nitrate reduction in a novel archaeal lineage, *Nature*, 500, 567–570, <https://doi.org/10.1038/nature12375>, 2013.
- Hedges, J. I. and Stern, J. H.: Carbon and nitrogen determinations of carbonate-containing solids I, *Limnol. Oceanogr.*, 29, 657–663, <https://doi.org/10.4319/lo.1984.29.3.0657>, 1984.
- Hoffmann, J. J. L., Schneider von Deimling, J., Schröder, J. F., Schmidt, M., Held, P., Crutchley, G. J., Scholten, J., and Gorman, A. R.: Complex eyed pockmarks and submarine groundwater discharge revealed by acoustic data and sediment cores in Eckernförde Bay, SW Baltic Sea, *Geochem. Geophys. Geosyst.*, 21, e2019GC008825, <https://doi.org/10.1029/2019GC008825>, 2020.
- Hopmans, E. C., Weijers, J. W. H., Schefuß, E., Herfort, L., Sinninghe Damsté, J. S., and Schouten, S.: A novel proxy for terrestrial organic matter in sediments based on branched and isoprenoid tetraether lipids, *Earth Planet. Sc. Lett.*, 224, 107–116, <https://doi.org/10.1016/j.epsl.2004.05.012>, 2004.
- Hopmans, E. C., Schouten, S., and Sinninghe Damsté, J. S.: The effect of improved chromatography on GDGT-based palaeoproxies, *Org. Geochem.*, 93, 1–6, <https://doi.org/10.1016/j.orggeochem.2015.12.006>, 2016.
- Hovland, M. and Judd, A. G.: *Seabed Pockmarks and Seepages. Impact on Geology, Biology and the Marine Environment*, Graham & Trotman (Kluwer), London, Dordrecht, Boston, 293 pp., ISBN 9780860109488, 1988.
- Hovland, M., Gardner, J. V., and Judd, A. G.: The significance of pockmarks to understanding fluid flow processes and geohazards, *Geofluids*, 2, 127–136, 2002.
- Huguet, A., Fosse, C., Laggoun-Défarge, F., Toussaint, M.-L., and Derenne, S.: Occurrence and distribution of glycerol dialkyl glycerol tetraethers in a French peat bog, *Org. Geochem.*, 41, 559–572, <https://doi.org/10.1016/j.orggeochem.2010.02.015>, 2010.
- Huguet, C., Hopmans, E. C., Febo-Ayala, W., Thompson, D. H., Sinninghe Damsté, J. S., and Schouten, S.: An improved method to determine the absolute abundance of glycerol dibiphy-

- tanyl glycerol tetraether lipids, *Org. Geochem.*, 37, 1036–1041, <https://doi.org/10.1016/j.orggeochem.2006.05.008>, 2006.
- Huguet, C., Fietz, S., and Rosell-Melé, A.: Global distribution patterns of hydroxy glycerol dialkyl glycerol tetraethers, *Org. Geochem.*, 57, 107–118, <https://doi.org/10.1016/j.orggeochem.2013.01.010>, 2013.
- Idczak, J., Brodecka-Goluch, A., Łukawska-Matuszewska, K., Graca, B., Gorska, N., Klusek, Z., Pezacki, P. D., and Bolałek, J.: A geophysical, geochemical and microbiological study of a newly discovered pockmark with active gas seepage and submarine groundwater discharge (MET1-BH, central Gulf of Gdańsk, southern Baltic Sea), *Sci. Tot. Environ.*, 742, 140306, <https://doi.org/10.1016/j.scitotenv.2020.140306>, 2020.
- Inglis, G. N., Farnsworth, A., Lunt, D., Foster, G. L., Hollis, C. J., Pagani, M., Jardine, P. E., Pearson, P. N., Markwick, P., Galsworthy, A. M. J., Raynham, L., Taylor, Kyle. W. R., and Pancost, R. D.: Descent toward the Icehouse: Eocene sea surface cooling inferred from GDGT distributions, *Paleoceanography*, 30, 1000–1020, <https://doi.org/10.1002/2014PA002723>, 2015.
- Ininbergs, K., Bergman, B., Larsson, J., and Ekman, M.: Microbial metagenomics in the Baltic Sea: Recent advancements and prospects for environmental monitoring, *AMBIO*, 44, 439–450, <https://doi.org/10.1007/s13280-015-0663-7>, 2015.
- Jakobs, G., Labrenz, M., Rehder, G., Hietanen, S., Kießlich, K., Vogts, A., Blumenberg, M., and Schmale, O.: A boreactor approach to investigate the linkage between methane oxidation and nitrate/nitrite reduction in the pelagic oxic-anoxic transition zone of the Central Baltic Sea, *Front. Mar. Sci.*, 3, <https://doi.org/10.3389/fmars.2016.00145>, 2016.
- Jakobsson, M., O'Regan, M., Mörth, C.-M., Stranne, C., Weidner, E., Hansson, J., Gyllencreutz, R., Humborg, C., Elfving, T., Norkko, A., Norkko, J., Nilsson, B., and Sjöström, A.: Potential links between Baltic Sea submarine terraces and groundwater seeping, *Earth Surf. Dyn.*, 8, 1–15, <https://doi.org/10.5194/esurf-8-1-2020>, 2020.
- Jääntti, H., Ward, B. B., Dippner, J. W., and Hietanen, S.: Nitrification and the ammonia-oxidizing communities in the central Baltic Sea water column, *Estuar. Coast. Shelf Sci.*, 202, 280–289, <https://doi.org/10.1016/j.ecss.2018.01.019>, 2018.
- Jaśniewicz, D., Klusek, Z., Brodecka-Goluch, A., and Bolałek, J.: Acoustic investigations of shallow gas in the southern Baltic Sea (Polish Exclusive Economic Zone): a review, *Geo-Mar. Lett.*, 39, 1–17, <https://doi.org/10.1007/s00367-018-0555-5>, 2019.
- Jaworowski, K., Wagner, R., Modliski, Z., Pokorski, J., Sokołowski, J., and Sokołowski, A.: Marine ecogeology in semi-closed basin: case study on a threat of geogenic pollution of the southern Baltic Sea (Polish Exclusive Economic Zone), *Geol. Q.*, 54, 267–288, 2010.
- Jensen, J. B., Kuijpers, A., Bennike, O., Laier, T., and Werner, F.: New geological aspects for freshwater seepage and formation in Eckernförde Bay, western Baltic, *Cont. Shelf Res.*, 22, 2159–2173, [https://doi.org/10.1016/S0278-4343\(02\)00076-6](https://doi.org/10.1016/S0278-4343(02)00076-6), 2002.
- Jørgensen, B. B.: Sulfur biogeochemical cycle of marine sediments, *Geochem. Perspect.*, 10, 145–146, 2021.
- Jørgensen, B. B., Weber, A., and Zopf, J.: Sulfate reduction and anaerobic methane oxidation in Black Sea sediments, *Deep-Sea Res. Part I Oceanogr. Res. Pap.*, 48, 2097–2120, [https://doi.org/10.1016/S0967-0637\(01\)00007-3](https://doi.org/10.1016/S0967-0637(01)00007-3), 2001.
- Justice, N. B., Szczesnak, A., Hazen, T. C., and Arkin, A. P.: Environmental selection, dispersal, and organism interactions shape community assembly in high-throughput enrichment culturing, *Appl. Environ. Microbiol.*, 83, e01253-17, <https://doi.org/10.1128/AEM.01253-17>, 2017.
- Kaiser, J. and Arz, H. W.: Sources of sedimentary biomarkers and proxies with potential paleoenvironmental significance for the Baltic Sea, *Cont. Shelf Res.*, 122, 102–119, <https://doi.org/10.1016/j.csr.2016.03.020>, 2016.
- Kapustina, M., Bubnova, E., and Dudkov, I.: Deep water of the Gdansk Deep (Baltic Sea): variability of hydrology and dissolved oxygen over recent decades, *Reg. Stud. Mar. Sci.*, 93, 104727, <https://doi.org/10.1016/j.risma.2025.104727>, 2026.
- Kim, B. and Zhang, Y. G.: Methane Index: Towards a quantitative archaeal lipid biomarker proxy for reconstructing marine sedimentary methane fluxes, *Geochim. Cosmochim. Acta*, 354, 74–87, <https://doi.org/10.1016/j.gca.2023.06.008>, 2023.
- King, L. H. and MacLean, B.: Pockmarks on the Scotian Shelf, *GSA Bulletin*, 81, 3141–3148, 1970.
- Knittel, K. and Boetius, A.: Anaerobic oxidation of methane: progress with an unknown process, *Annu. Rev. Microbiol.*, 63, 311–334, <https://doi.org/10.1146/annurev.micro.61.080706.093130>, 2009.
- Koga, Y., Nishihara, M., Morii, H., and Akagawa-Matsushita, M.: Ether polar lipids of methanogenic bacteria: structures, comparative aspects, and biosyntheses, *Microbiol. Rev.*, 57, 164–182, <https://doi.org/10.1128/mr.57.1.164-182.1993>, 1993.
- Kotarba, M. J.: Origin of hydrocarbon gases accumulated in the Middle Cambrian reservoirs of the Polish part of the Baltic region, *Geol. Q.*, 54, 197–204, 2010.
- Kotarba, M. J. and Lewan, M. D.: Sources of natural gases in Middle Cambrian reservoirs in Polish and Lithuanian Baltic Basin as determined by stable isotopes and hydrous pyrolysis of Lower Palaeozoic source rocks, *Chem. Geol.*, 345, 62–76, <https://doi.org/10.1016/j.chemgeo.2013.02.023>, 2013.
- Kotarba, M. J. and Nagao, K.: Molecular and isotopic compositions and origin of natural gases from Cambrian and Carboniferous-Lower Permian reservoirs of the onshore Polish Baltic region, *Int. J. Earth Sci.*, 104, 241–261, <https://doi.org/10.1007/s00531-014-1063-0>, 2015.
- Kreuzburg, M., Scholten, J., Hsu, F.-H., Liebetrau, V., Sültenfuß, J., Rapaglia, J., and Schlüter, M.: Submarine groundwater discharge-derived nutrient fluxes in Eckernförde Bay (Western Baltic Sea), *Estuaries Coasts*, 46, 1190–1207, <https://doi.org/10.1007/s12237-023-01202-0>, 2023.
- Kuliński, K., Rehder, G., Asmala, E., Bartosova, A., Carstensen, J., Gustafsson, B., Hall, P. O. J., Humborg, C., Jilbert, T., Jürgens, K., Meier, H. E. M., Müller-Karulis, B., Naumann, M., Olesen, J. E., Savchuk, O., Schramm, A., Slomp, C. P., Sofiev, M., Sobek, A., Szymczycha, B., and Undeman, E.: Biogeochemical functioning of the Baltic Sea, *Earth Syst. Dyn.*, 13, 633–685, <https://doi.org/10.5194/esd-13-633-2022>, 2022.
- Kurowski, S., Łukawska-Matuszewska, K., Čović, A., Jozić, D., and Brodecka-Goluch, A.: Effects of pockmark activity on iron cycling and mineral composition in continental shelf sediments (southern Baltic Sea), *Biogeochemistry*, 167, 135–154, <https://doi.org/10.1007/s10533-024-01127-1>, 2024.

- Labrenz, M., Sintes, E., Toetzke, F., Zumsteg, A., Herndl, G. J., Seidler, M., and Jürgens, K.: Relevance of a crenarchaeotal subcluster related to *Candidatus Nitrosopumilus maritimus* to ammonia oxidation in the suboxic zone of the central Baltic Sea, *ISME J.*, 4, 1496–1508, <https://doi.org/10.1038/ismej.2010.78>, 2010.
- Lapham, L. L., Lloyd, K. G., Fossing, H., Flury, S., Jensen, J. B., Alperin, M. J., Rehder, G., Holzhueter, W., Ferdelman, T., and Jørgensen, B. B.: Methane leakage through the sulfate–methane transition zone of the Baltic seabed, *Nat. Geosci.*, 17, 1277–1283, <https://doi.org/10.1038/s41561-024-01594-z>, 2024.
- Lawal, M. A., Cook, A. E., Portnov, A., and Kumar, A.: Pockmarks, mud volcanoes and hydrocarbon seeps in the Northern Gulf of Mexico: trends and controls on widespread fluid and gas venting, *Basin Res.*, 38, e70095, <https://doi.org/10.1111/bre.70095>, 2026.
- Lee, D.-H., Kim, J.-H., Lee, Y. M., Stadnitskaia, A., Jin, Y. K., Niemann, H., Kim, Y.-G., and Shin, K.-H.: Biogeochemical evidence of anaerobic methane oxidation on active submarine mud volcanoes on the continental slope of the Canadian Beaufort Sea, *Biogeosciences*, 15, 7419–7433, <https://doi.org/10.5194/bg-15-7419-2018>, 2018.
- Lengger, S. K., Kraaij, M., Tjallingii, R., Baas, M., Stuut, J.-B., Hopmans, E. C., Sinninghe Damsté, J. S., and Schouten, S.: Differential degradation of intact polar and core glycerol dialkyl glycerol tetraether lipids upon post-depositional oxidation, *Org. Geochem.*, 65, 83–93, <https://doi.org/10.1016/j.orggeochem.2013.10.004>, 2013.
- Leu, A. O., Cai, C., McIlroy, S. J., Southam, G., Orphan, V. J., Yuan, Z., Hu, S., and Tyson, G. W.: Anaerobic methane oxidation coupled to manganese reduction by members of the Methanoperedenaceae, *ISME J.*, 14, 1030–1041, <https://doi.org/10.1038/s41396-020-0590-x>, 2020.
- Li, X., Li, Y., Gao, D., Liu, M., and Hou, L.: Methane production linked to organic matter molecule and methanogenic community in estuarine benthic sediments, *J. Geophys. Res. Biogeosci.*, 127, e2022JG007236, <https://doi.org/10.1029/2022JG007236>, 2022.
- Liu, Q., Charette, M. A., Breier, C. F., Henderson, P. B., McCorkle, D. C., Martin, W., and Dai, M.: Carbonate system biogeochemistry in a subterranean estuary – Waquoit Bay, USA, *Geochim. Cosmochim. Acta*, 203, 422–439, <https://doi.org/10.1016/j.gca.2017.01.041>, 2017.
- Liu, X.-L., Summons, R. E., and Hinrichs, K.-U.: Extending the known range of glycerol ether lipids in the environment: structural assignments based on tandem mass spectral fragmentation patterns, *Rapid Commun. Mass Spectrom.*, 26, 2295–2302, <https://doi.org/10.1002/rcm.6355>, 2012.
- Lu, J., Breitwieser, F. P., Thielen, P., and Salzberg, S. L.: Bracken: estimating species abundance in metagenomics data, *PeerJ Computer Sci.*, 3, e104, <https://doi.org/10.7717/peerj-cs.104>, 2017.
- Lu, J., Rincon, N., Wood, D. E., Breitwieser, F. P., Pockrandt, C., Langmead, B., Salzberg, S. L., and Steinegger, M.: Metagenome analysis using the Kraken software suite, *Nat. Protoc.*, 17, 2815–2839, <https://doi.org/10.1038/s41596-022-00738-y>, 2022.
- Lü, X., Liu, X.-L., Elling, F. J., Yang, H., Xie, S., Song, J., Li, X., Yuan, H., Li, N., and Hinrichs, K.-U.: Hydroxylated isoprenoid GDGTs in Chinese coastal seas and their potential as a paleotemperature proxy for mid-to-low latitude marginal seas, *Org. Geochem.*, 89–90, 31–43, <https://doi.org/10.1016/j.orggeochem.2015.10.004>, 2015.
- Łukawska-Matuszewska, K.: Contribution of non-carbonate inorganic and organic alkalinity to total measured alkalinity in pore waters in marine sediments (Gulf of Gdansk, S-E Baltic Sea), *Mar. Chem.*, 186, 211–220, <https://doi.org/10.1016/j.marchem.2016.10.002>, 2016.
- Łukawska-Matuszewska, K. and Dwornik, M.: Early diagenesis in anoxic sediments of the Gulf of Gdańsk (southern Baltic Sea): Implications for porewater chemistry and benthic flux of carbonate alkalinity, *Front. Earth Sci.*, 13, <https://doi.org/10.3389/feart.2025.1593031>, 2025.
- Łukawska-Matuszewska, K., Kiełczewska, J., and Bolałek, J.: Factors controlling spatial distributions and relationships of carbon, nitrogen, phosphorus and sulphur in sediments of the stratified and eutrophic Gulf of Gdansk, *Cont. Shelf Res.*, 85, 168–180, <https://doi.org/10.1016/j.csr.2014.06.010>, 2014.
- Łukawska-Matuszewska, K., Broclawik, O., Brodecka-Goluch, A., Rzepa, G., Manecki, M., and Bolałek, J.: Biogeochemical and mineralogical effects of Fe-P-S dynamics in sediments of continental shelf sea: Impact of salinity, oxygen conditions, and catchment area characteristics, *Sci. Tot. Environ.*, 807, 151035, <https://doi.org/10.1016/j.scitotenv.2021.151035>, 2022.
- Łukawska-Matuszewska, K., Brodecka-Goluch, A., Czachor, A., and Rios-Quintero, R.: Gas bubble release areas as new potential hot spots for water column enrichment with nutrients in eutrophicated sea, *Mar. Environ. Res.*, 205, 106981, <https://doi.org/10.1016/j.marenvres.2025.106981>, 2025.
- Lundsten, E., Paull, C. K., Gwiazda, R., Dobbs, S., Caress, D. W., Kuhn, L. A., Walton, M., Nieminski, N., McGann, M., Lorenson, T., Cochrane, G., and Addison, J.: Pockmarks offshore Big Sur, California provide evidence for recurrent, regional, and unconfined sediment gravity flows, *J. Geophys. Res. Earth Surf.*, 129, e2023JF007374, <https://doi.org/10.1029/2023JF007374>, 2024.
- Lynes, M. M., Jay, Z. J., Kohtz, A. J., and Hatzenpichler, R.: Methylophilic methanogenesis in the Archaeoglobi revealed by cultivation of *Ca. Methanoglobus hypatiae* from a Yellowstone hot spring, *ISME J.*, 18, wrae026, <https://doi.org/10.1093/ismejo/wrae026>, 2024.
- Maeder, D. L., Anderson, I., Brettin, T. S., Bruce, D. C., Gilna, P., Han, C. S., Lapidus, A., Metcalf, W. W., Saunders, E., Tapia, R., and Sowers, K. R.: The *Methanosarcina barkeri* genome: comparative analysis with *Methanosarcina acetivorans* and *Methanosarcina mazei* reveals extensive rearrangement within methanosarcinal genomes, *J. Bacteriol.*, 188, 7922–7931, <https://doi.org/10.1128/JB.00810-06>, 2006.
- Majewski, P. and Klusek, Z.: Expressions of shallow gas in the Gdansk Basin, *Sci. J. Polish Nav. Acad.*, 52, 61–71, 2011.
- Martens-Habbena, W. and Qin, W.: Archaeal nitrification without oxygen, *Science*, 375, 27–28, <https://doi.org/10.1126/science.abn0373>, 2022.
- Moore, W. S.: The subterranean estuary: a reaction zone of ground water and sea water, *Mar. Chem.*, 65, 111–125, [https://doi.org/10.1016/S0304-4203\(99\)00014-6](https://doi.org/10.1016/S0304-4203(99)00014-6), 1999.
- Moore, W. S.: The effect of submarine groundwater discharge on the ocean, *Annu. Rev. Mar. Sci.*, 2, 59–88, <https://doi.org/10.1146/annurev-marine-120308-081019>, 2010.
- Niemann, H. and Elvert, M.: Diagnostic lipid biomarker and stable carbon isotope signatures of microbial communities mediating the anaerobic oxidation of

- methane with sulphate, *Org. Geochem.*, 39, 1668–1677, <https://doi.org/10.1016/j.orggeochem.2007.11.003>, 2008.
- O'Reilly, S. S., Jordan, S. F., Monteys, X., Simpson, A. J., Allen, C. C. R., Szpak, M. T., Murphy, B. T., McCarron, S. G., Soong, R., Wu, B., Jenne, A., Grey, A., and Kelleher, B. P.: Production of methane and gaseous compounds by surface microbial activity in a small pockmark field, Dunmanus Bay, Ireland, *Estuar. Coast. Shelf Sci.*, 255, 107340, <https://doi.org/10.1016/j.ecss.2021.107340>, 2021.
- Palarea-Albaladejo, J. and Martín-Fernández, J. A.: zCompositions – R package for multivariate imputation of left-censored data under a compositional approach, *Chemometr. Intell. Lab.*, 143, 85–96, <https://doi.org/10.1016/j.chemolab.2015.02.019>, 2015.
- Pancost, R. D., Hopmans, E. C., and Sinninghe Damsté, J. S.: Archaeal lipids in Mediterranean cold seeps: molecular proxies for anaerobic methane oxidation, *Geochim. Cosmochim. Acta*, 65, 1611–1627, [https://doi.org/10.1016/S0016-7037\(00\)00562-7](https://doi.org/10.1016/S0016-7037(00)00562-7), 2001.
- Parsons, T. R., Maita, Y., and Lalli, C. M.: *A Manual of Chemical & Biological Methods for Seawater Analysis*, Pergamon Press, 188 pp., ISBN 0-08-030288-2, 1984.
- Peterse, F., Kim, J.-H., Schouten, S., Kristensen, D. K., Koç, N., and Sinninghe Damsté, J. S.: Constraints on the application of the MBT/CBT palaeothermometer at high latitude environments (Svalbard, Norway), *Org. Geochem.*, 40, 692–699, <https://doi.org/10.1016/j.orggeochem.2009.03.004>, 2009.
- Petrick, B., Reuning, L., and Martínez-García, A.: Distribution of glycerol dialkyl glycerol tetraethers (GDGTs) in microbial mats from Holocene and Miocene sabkha sediments, *Front. Earth Sci.*, 7, <https://doi.org/10.3389/feart.2019.00310>, 2019.
- Piekarek-Jankowska, H.: Hydrochemical effects of submarine groundwater discharge to the Puck Bay [Southern Baltic Sea, Poland], *Geogr. Pol.*, 67, 103–119, 1996.
- Pimenov, N. V., Ulyanova, M. O., Kanapatsky, T. A., Veslopolova, E. F., Sigalevich, P. A., and Sivkov, V. V.: Microbially mediated methane and sulfur cycling in pockmark sediments of the Gdansk Basin, Baltic Sea, *Geo-Mar. Lett.*, 30, 439–448, <https://doi.org/10.1007/s00367-010-0200-4>, 2010.
- Pokorski, J.: Geological section through the lower Paleozoic strata of the Polish part of the Baltic region, *Geol. Q.*, 54, 123–130, 2010.
- Purkamo, L., von Ahn, C. M. E., Jilbert, T., Muniruz-zaman, M., Bange, H. W., Jenner, A.-K., Böttcher, M. E., and Virtasalo, J. J.: Impact of submarine groundwater discharge on biogeochemistry and microbial communities in pockmarks, *Geochim. Cosmochim. Acta*, 334, 14–44, <https://doi.org/10.1016/j.gca.2022.06.040>, 2022.
- Quast, C., Pruesse, E., Yilmaz, P., Gerken, J., Schweer, T., Yarza, P., Peplies, J., and Glöckner, F. O.: The SILVA ribosomal RNA gene database project: improved data processing and web-based tools, *Nucleic Acids Res.*, 41, D590–D596, <https://doi.org/10.1093/nar/gks1219>, 2013.
- Quinn, T. P., Erb, I., Gloor, G., Notredame, C., Richardson, M. F., and Crowley, T. M.: A field guide for the compositional analysis of any-omics data, *GigaScience*, 8, giz107, <https://doi.org/10.1093/gigascience/giz107>, 2019.
- R Core Team: R: A Language and Environment for Statistical Computing. R Foundation for Statistical Computing, Vienna, <https://www.R-project.org> (last access: 1 July 2026), 2022.
- Reeburgh, W. S.: Oceanic methane biogeochemistry, *Chem. Rev.*, 107, 486–513, <https://doi.org/10.1021/cr050362v>, 2007.
- Rinke, C., Chuvochina, M., Mussig, A. J., Chaumeil, P.-A., Davín, A. A., Waite, D. W., Whitman, W. B., Parks, D. H., and Hugenholtz, P.: A standardized archaeal taxonomy for the Genome Taxonomy Database, *Nat. Microbiol.*, 6, 946–959, <https://doi.org/10.1038/s41564-021-00918-8>, 2021.
- Roberts, H. H. and Aharon, P.: Hydrocarbon-derived carbonate buildups of the northern Gulf of Mexico continental slope: A review of submersible investigations, *Geo-Mar. Lett.*, 14, 135–148, <https://doi.org/10.1007/BF01203725>, 1994.
- Rogers, D. R. and Casciotti, K. L.: Abundance and diversity of archaeal ammonia oxidizers in a coastal groundwater system, *Applied and Environ. Microbiol.*, 76, 7938–7948, <https://doi.org/10.1128/AEM.02056-09>, 2010.
- Rossel, P. E., Lipp, J. S., Fredricks, H. F., Arnds, J., Boetius, A., Elvert, M., and Hinrichs, K.-U.: Intact polar lipids of anaerobic methanotrophic archaea and associated bacteria, *Org. Geochem.*, 39, 992–999, <https://doi.org/10.1016/j.orggeochem.2008.02.021>, 2008.
- Ruiz-González, C., Rodellas, V., and Garcia-Orellana, J.: The microbial dimension of submarine groundwater discharge: current challenges and future directions, *FEMS Microbiol. Rev.*, 45, fuab010, <https://doi.org/10.1093/femsre/fuab010>, 2021.
- Rzepa, G., Borkowski, A., Manecki, M., Brodecka-Goluch, A., Łukawska-Matuszewska, K., Kania, J., Błachowski, A., and De Mey-Śnieżyńska, I.: The effect of freshwater discharge on the microbial-induced precipitation of minerals in a Baltic Sea bottom pockmark, *Oceanologia*, <https://doi.org/10.5697/NDCH3019>, 2026.
- Santoro, A. E., Francis, C. A., De Sienes, N. R., and Boehm, A. B.: Shifts in the relative abundance of ammonia-oxidizing bacteria and archaea across physicochemical gradients in a subterranean estuary, *Environ. Microbiol.*, 10, 1068–1079, <https://doi.org/10.1111/j.1462-2920.2007.01547.x>, 2008.
- Schlüter, M., Sauter, E. J., Andersen, C. E., Dahlgaard, H., and Dando, P. R.: Spatial distribution and budget for submarine groundwater discharge in Eckernförde Bay (Western Baltic Sea), *Limnol. Oceanogr.*, 49, 157–167, <https://doi.org/10.4319/lo.2004.49.1.0157>, 2004.
- Schmale, O., Schneider von Deimling, J., Gülzow, W., Nausch, G., Waniek, J. J., and Rehder, G.: Distribution of methane in the water column of the Baltic Sea, *Geophys. Res. Lett.*, 37, <https://doi.org/10.1029/2010GL043115>, 2010.
- Schmuck, E. A. and Paull, C. K.: Evidence for gas accumulation associated with diapirism and gas hydrates at the head of the Cape Fear Slide, *Geo-Mar. Lett.*, 13, 145–152, <https://doi.org/10.1007/BF01593187>, 1993.
- Schouten, S., Hopmans, E. C., Schefuß, E., and Sinninghe Damsté, J. S.: Distributional variations in marine crenarchaeotal membrane lipids: a new tool for reconstructing ancient sea water temperatures?, *Earth Planet. Sc. Lett.*, 204, 265–274, [https://doi.org/10.1016/S0012-821X\(02\)00979-2](https://doi.org/10.1016/S0012-821X(02)00979-2), 2002.
- Schouten, S., Hopmans, E. C., and Sinninghe Damsté, J. S.: The organic geochemistry of glycerol dialkyl glycerol tetraether lipids: A review, *Org. Geochem.*, 54, 19–61, <https://doi.org/10.1016/j.orggeochem.2012.09.006>, 2013.
- Shaw, J., Courtney, R. C., and Currie, J. R.: Marine geology of St. George's Bay, Newfoundland, as interpreted from multibeam

- bathymetry and back-scatter data, *Geo-Mar. Lett.*, 17, 188–194, <https://doi.org/10.1007/s003670050025>, 1997.
- Sinninghe Damsté, J. S., Schouten, S., Hopmans, E. C., Duin, A. C. T. van, and Geenevasen, J. A. J.: Crenarchaeol, *J. Lipid Res.*, 43, 1641–1651, <https://doi.org/10.1194/jlr.M200148-JLR200>, 2002.
- Sinninghe Damsté, J. S., Warden, L. A., Berg, C., Jürgens, K., and Moros, M.: Evaluation of the distributions of hydroxylated glycerol dibiphytanyl glycerol tetraethers (GDGTs) in Holocene Baltic Sea sediments for reconstruction of sea surface temperature: the effect of changing salinity, *Clim. Past*, 18, 2271–2288, <https://doi.org/10.5194/cp-18-2271-2022>, 2022.
- Słowakiewicz, M., Whitaker, F., Thomas, L., Tucker, M. E., Zheng, Y., Gedl, P., and Pancost, R. D.: Biogeochemistry of intertidal microbial mats from Qatar: New insights from organic matter characterisation, *Org. Geochem.*, 102, 14–29, <https://doi.org/10.1016/j.orggeochem.2016.09.006>, 2016.
- Sowers, K. R., Boone, J. E., and Gunsalus, R. P.: Disaggregation of *Methanosarcina* spp. and growth as single cells at elevated osmolarity, *Applied and Environ. Microbiol.*, 59, 3832–3839, <https://doi.org/10.1128/aem.59.11.3832-3839.1993>, 1993.
- Stadnitskaia, A., Muyzer, G., Abbas, B., Coolen, M. J. L., Hopmans, E. C., Baas, M., van Weering, T. C. E., Ivanov, M. K., Poludetkina, E., and Sinninghe Damsté, J. S.: Biomarker and 16S rDNA evidence for anaerobic oxidation of methane and related carbonate precipitation in deep-sea mud volcanoes of the Sorokin Trough, Black Sea, *Mar. Geol.*, 217, 67–96, <https://doi.org/10.1016/j.margeo.2005.02.023>, 2005.
- Szczepańska, T. and Uścińowicz, S.: Atlas geochemiczny południowego Bałtyku, Państwowy Instytut Geologiczny, Warszawa, 1–55, 1994.
- Szymczak-Żyła, M. and Lubecki, L.: Biogenic and anthropogenic sources of sedimentary organic matter in marine coastal areas: A multi-proxy approach based on bulk and molecular markers, *Mar. Chem.*, 239, 104069, <https://doi.org/10.1016/j.marchem.2021.104069>, 2022.
- Szymczycha, B., Kroeger, K. D., and Pempkowiak, J.: Significance of groundwater discharge along the coast of Poland as a source of dissolved metals to the southern Baltic Sea, *Mar. Pollut. Bull.*, 109, 151–162, <https://doi.org/10.1016/j.marpolbul.2016.06.008>, 2016.
- Szymczycha, B., Kłostowska, Ż., Kuliński, K., Winogradow, A., Jakacki, J., Klusek, Z., Grabowski, M., Brodecka-Goluch, A., Graca, B., Stokowski, M., Kozirowska, K., and Rak, D.: Deep submarine groundwater discharge indicated by pore water chloride anomalies in the Gulf of Gdańsk, southern Baltic Sea, *E3S Web of Conferences*, 54, 00035, <https://doi.org/10.1051/e3sconf/20185400035>, 2018.
- Taniguchi, M., Dulai, H., Burnett, K. M., Santos, I. R., Sugimoto, R., Stieglitz, T., Kim, G., Moosdorf, N., and Burnett, W. C.: Submarine groundwater discharge: updates on its measurement techniques, geophysical drivers, magnitudes, and effects, *Front. Environ. Sci.*, 7, <https://doi.org/10.3389/fenvs.2019.00141>, 2019.
- Taylor, M. H., Dillon, W. P., and Pecher, I. A.: Trapping and migration of methane associated with the gas hydrate stability zone at the Blake Ridge Diapir: new insights from seismic data, *Mar. Geol.*, 164, 79–89, [https://doi.org/10.1016/S0025-3227\(99\)00128-0](https://doi.org/10.1016/S0025-3227(99)00128-0), 2000.
- Treude, T., Nigemann, J., Kallmeyer, J., Wintersteller, P., Schubert, C. J., Boetius, A., and Jørgensen, B. B.: Anaerobic oxidation of methane and sulfate reduction along the Chilean continental margin, *Geochim. Cosmochim. Acta*, 69, 2767–2779, <https://doi.org/10.1016/j.gca.2005.01.002>, 2005.
- Uścińowicz, S. (Ed.): *Geochemistry of Baltic Sea surface sediments*, Polish Geological Institute – National Research Institute, Warsaw, 356 pp., ISBN 978-83-7538-814-5, 2011.
- Vaksmaa, A., Guerrero-Cruz, S., van Alen, T. A., Cremers, G., Ettwig, K. F., Lüke, C., and Jetten, M. S. M.: Enrichment of anaerobic nitrate-dependent methanotrophic ‘*Candidatus Methanoperedens nitroreducens*’ archaea from an Italian paddy field soil, *Appl. Microbiol. Biotechnol.*, 101, 7075–7084, <https://doi.org/10.1007/s00253-017-8416-0>, 2017.
- van den Boogaart, K. G., Tolosana-Delgado, R., and Bren, M.: Package “compositions”: Compositional Data Analysis, <https://doi.org/10.32614/CRAN.package.compositions>, 2024.
- Varma, D., Hopmans, E. C., van Kemenade, Z. R., Kusch, S., Berg, S., Bale, N. J., Sangiorgi, F., Reichart, G.-J., Sinninghe Damsté, J. S., and Schouten, S.: Evaluating isoprenoidal hydroxylated GDGT-based temperature proxies in surface sediments from the global ocean, *Geochim. Cosmochim. Acta*, 370, 113–127, <https://doi.org/10.1016/j.gca.2023.12.019>, 2024.
- Virtasalo, J. J., Schröder, J. F., Luoma, S., Majaniemi, J., Mursu, J., and Scholten, J.: Submarine groundwater discharge site in the First Salpausselkä ice-marginal formation, south Finland, *Solid Earth*, 10, 405–423, <https://doi.org/10.5194/se-10-405-2019>, 2019.
- Wakeham, S. G., Lewis, C. M., Hopmans, E. C., Schouten, S., and Sinninghe Damsté, J. S.: Archaea mediate anaerobic oxidation of methane in deep euxinic waters of the Black Sea, *Geochim. Cosmochim. Acta*, 67, 1359–1374, [https://doi.org/10.1016/S0016-7037\(02\)01220-6](https://doi.org/10.1016/S0016-7037(02)01220-6), 2003.
- Waters, E., Hohn, M. J., Ahel, I., Graham, D. E., Adams, M. D., Barnstead, M., Beeson, K. Y., Bibbs, L., Bolanos, R., Keller, M., Kretz, K., Lin, X., Mathur, E., Ni, J., Podar, M., Richardson, T., Sutton, G. G., Simon, M., Söll, D., Stetter, K. O., Short, J. M., and Noordewier, M.: The genome of *Nanoarchaeum equitans*: Insights into early archaeal evolution and derived parasitism, *Proc. Natl. Acad. Sci. USA*, 100, 12984–12988, <https://doi.org/10.1073/pnas.1735403100>, 2003.
- Weijers, J. W. H., Schouten, S., Hopmans, E. C., Geenevasen, J. A. J., David, O. R. P., Coleman, J. M., Pancost, R. D., and Sinninghe Damsté, J. S.: Membrane lipids of mesophilic anaerobic bacteria thriving in peats have typical archaeal traits, *Environ. Microbiol.*, 8, 648–657, <https://doi.org/10.1111/j.1462-2920.2005.00941.x>, 2006.
- Weijers, J. W. H., Lim, K. L. H., Aquilina, A., Sinninghe Damsté, J. S., and Pancost, R. D.: Biogeochemical controls on glycerol dialkyl glycerol tetraether lipid distributions in sediments characterized by diffusive methane flux, *Geochim. Geophys. Geosyst.*, 12, 1–15, <https://doi.org/10.1029/2011GC003724>, 2011.
- Welte, C., Kröninger, L., and Deppenmeier, U.: Experimental evidence of an acetate transporter protein and characterization of acetate activation in aceticlastic methanogenesis of *Methanosarcina mazei*, *FEMS Microbiol. Lett.*, 359, 147–153, <https://doi.org/10.1111/1574-6968.12550>, 2014.
- Werner, F.: Depressions in mud sediments (Eckernförde Bay, Baltic Sea), related to sub-bottom and currents, *Meyniana*, 30, 99–104, 1978.

- Wever, Th. F., Abegg, F., Fiedler, H. M., Fechner, G., and Stender, I. H.: Shallow gas in the muddy sediments of Eckernförde Bay, Germany, *Cont. Shelf Res.*, 18, 1715–1739, [https://doi.org/10.1016/S0278-4343\(98\)00055-7](https://doi.org/10.1016/S0278-4343(98)00055-7), 1998.
- Whiticar, M. J.: Diagenetic relationships of methanogenesis, nutrients, acoustic turbidity, pockmarks and freshwater seepages in Eckernförde Bay, *Mar. Geol.*, 182, 29–53, [https://doi.org/10.1016/S0025-3227\(01\)00227-4](https://doi.org/10.1016/S0025-3227(01)00227-4), 2002.
- Whiticar, M. J. and Werner, F.: Pockmarks: Submarine vents of natural gas or freshwater seeps?, *Geo-Mar. Lett.*, 1, 193–199, <https://doi.org/10.1007/BF02462433>, 1981.
- Wickham, H.: *ggplot2: Elegant Graphics for Data Analysis*, Springer International Publishing, 260, https://doi.org/10.1007/978-3-319-24277-4_9, 2016.
- Wilson, S. J., Song, B., Anderson, I. C., and Tobias, C. R.: Nitrification in a subterranean estuary: An ex situ and in situ method comparison determines nitrate is available for discharge, *J. Geophys. Res. Biogeosci.*, 129, e2023JG007876, <https://doi.org/10.1029/2023JG007876>, 2024.
- Wittenborn, A. K., Bauersachs, T., Hassenrück, C., Käding, K., Wäge-Recchioni, J., Jürgens, K., Arz, H. W., and Kaiser, J.: Nitrosopumilus as main source of isoprenoid glycerol dialkyl glycerol tetraether lipids in the central Baltic Sea, *Front. Microbiol.*, 14, <https://doi.org/10.3389/fmicb.2023.1216130>, 2023.
- Wood, D. E., Lu, J., and Langmead, B.: Improved metagenomic analysis with Kraken 2, *Genome Biol.*, 20, 257, <https://doi.org/10.1186/s13059-019-1891-0>, 2019.
- Yi, X., Brandt, K. K., Xue, S., Peng, J., Wang, Y., Li, M., Deng, Y., and Duan, G.: Niche differentiation and biogeography of Bathyarchaeia in paddy soil ecosystems: a case study in eastern China, *Environ. Microbiome*, 19, 13, <https://doi.org/10.1186/s40793-024-00555-8>, 2024.
- Yu, T., Fu, L., Wang, Y., Dong, Y., Chen, Y., Wegener, G., Cheng, L., and Wang, F.: Thermophilic Hadarchaeota grow on long-chain alkanes in syntrophy with methanogens, *Nat. Commun.*, 15, 6560, <https://doi.org/10.1038/s41467-024-50883-z>, 2024.
- Zehnder, A. J. B. and Brock, T. D.: Anaerobic methane oxidation: occurrence and ecology, *Appl. Environ. Microbiol.*, 39, 194–204, <https://doi.org/10.1128/aem.39.1.194-204.1980>, 1980.
- Zell, C., Kim, J.-H., Hollander, D., Lorenzoni, L., Baker, P., Silva, C. G., Nittrouer, C., and Sinninghe Damsté, J. S.: Sources and distributions of branched and isoprenoid tetraether lipids on the Amazon shelf and fan: Implications for the use of GDGT-based proxies in marine sediments, *Geochim. Cosmochim. Acta*, 139, 293–312, <https://doi.org/10.1016/j.gca.2014.04.038>, 2014.
- Zeng, Z., Chen, H., Yang, H., Chen, Y., Yang, W., Feng, X., Pei, H., and Welander, P. V.: Identification of a protein responsible for the synthesis of archaeal membrane-spanning GDGT lipids, *Nat. Commun.*, 13, 1545, <https://doi.org/10.1038/s41467-022-29264-x>, 2022.
- Zhang, Y. G., Zhang, C. L., Liu, X.-L., Li, L., Hinrichs, K.-U., and Noakes, J. E.: Methane Index: A tetraether archaeal lipid biomarker indicator for detecting the instability of marine gas hydrates, *Earth Planet. Sci. Lett.*, 307, 525–534, <https://doi.org/10.1016/j.epsl.2011.05.031>, 2011.
- Zhang, Z., Shan, H., Feng, X., Jia, Z., Jiang, L., Wang, S., and Zhu, C.: Review of research progress on the impact of submarine groundwater discharge on pockmark formation and evolution, *J. Mar. Sci. Eng.*, 13, 1070, <https://doi.org/10.3390/jmse13061070>, 2025.
- Zhou, Z., Pan, J., Wang, F., Gu, J.-D., and Li, M.: Bathyarchaeota: globally distributed metabolic generalists in anoxic environments, *FEMS Microbiol. Rev.*, 42, 639–655, <https://doi.org/10.1093/femsre/fuy023>, 2018.
- Zinke, L. A., Glombitza, C., Bird, J. T., Røy, H., Jørgensen, B. B., Lloyd, K. G., Amend, J. P., and Reese, B. K.: Microbial organic matter degradation potential in Baltic Sea sediments is influenced by depositional conditions and in situ geochemistry, *Appl. Environ. Microbiol.*, 85, e02164-18, <https://doi.org/10.1128/AEM.02164-18>, 2019.